ACS OMEGA

http://pubs.acs.org/journal/acsodf

Article

Unique Compatibilized Thermoplastic Elastomer with High Strength and Remarkable Ductility: Effect of Multiple Point Interactions within a Rubber-Plastic Blend

Harekrishna Panigrahi, Paradesiparampil R. Sreenath, and Dinesh Kumar Kotnees*

Cite This: *ACS Omega* 2020, 5, 12789−12808

Read Online

ACCESS | Metrics & More | Article Recommendations

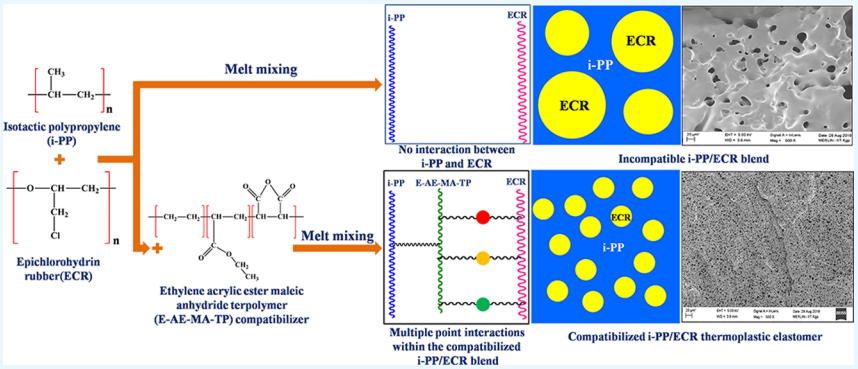

ABSTRACT: In the case of thermoplastic elastomers (TPEs) based on nonpolar polypropylene (PP) and polar rubbers, a small quantity of a third component known as the compatibilizer is added to maximize the compatibility between the incompatible blend components. Generally, one part of the compatibilizer reacts with the nonpolar PP phase and the other part of the compatibilizer reacts with the polar rubber phase, which in turn produces TPEs with useful properties. Till today, there have been no reports in the literature that examine the effect of a compatibilizer that can have multifaceted interactions with the incompatible blend components for the development of TPEs with unique properties. Accordingly, here, an ethylene-acrylic ester-maleic anhydride terpolymer (E-AE-MA-TP) has been used as the compatibilizer for the preparation of TPEs based on nonpolar isotactic polypropylene (i-PP) and polar epichlorohydrin rubber (ECR). The E-AE-MA-TP compatibilizer contains ethylene groups, acrylic groups, and anhydride/acid groups along its backbone, which act as the sites for establishing multifaceted interactions with both i-PP and ECR. The compatibilization efficiency of the E-AE-MA-TP compatibilizer has been analyzed by contact angle measurements, Fourier transform infrared (FTIR) spectroscopy, tensile stress−strain studies, mixing torque profiles, rheological studies, differential scanning calorimetry (DSC), field emission scanning electron microscopy (FESEM), and atomic force microscopy (AFM) images. The particle size of the dispersed ECR domains in the i-PP matrix of the i-PP/ECR blend prominently decreases (∼90% reduction) by incorporation of a very low dosage (5 wt %) of the E-AE-MA-TP compatibilizer. The i-PP/ECR (40 wt %/60 wt %) blend containing 5 wt % compatibilizer displays outstanding mechanical properties (especially strain at break value (∼370%)), which are superior to the mechanical properties of several compatibilized TPEs (based on PP and polar rubbers) reported in the literature. The unique properties of TPEs based on i-PP and ECR in the presence of the E-AE-MA-TP compatibilizer is attributed to the efficacy of the E-AE-MA-TP compatibilizer to establish multifaceted interactions with both i-PP and ECR.

1. INTRODUCTION

Thermoplastic elastomers (TPEs) are a unique class of polymers that combines the features of both elastomers and thermoplastics.[1−6] TPEs are biphasic materials, where one phase is soft and rubbery and the other phase is hard and glassy-amorphous or has a semicrystalline nature.[2,3] Therefore, TPEs exhibit properties that are similar to rubbery materials but can be melt-processed like typical thermoplastics.[1,3] TPEs are generally prepared by a melt mixing process in which the semicrystalline plastics are melted and combined with the desired amount of elastomers using an internal mixer or extruder.[4,5] The high shear stress and temperature associated with the melt mixing process of TPEs can result in well-

Received: January 30, 2020
Accepted: May 18, 2020
Published: May 26, 2020

dispersed rubber domains with good homogeneity in size throughout the continuous plastic matrix.[4,5] Generally, the melt mixing process is widely used for the preparation of TPEs because this process is cost-effective, does not involve usage of any solvents, and is suitable for commercial production.[4,5] It should be pointed out here that the rubber−plastic blends fall under the category of TPEs only when they inherit certain important features of rubbers like high elongation (>100%) and low tension set (<50%) properties.[6] In the past few years, PP-based TPEs have gathered increased attention since they have shown great potential for commercialization (i.e., industrial and commodity applications).[6,7] There are a number of reports in the literature that investigate the preparation of PP-based TPEs by directly mixing PP with various compatible nonpolar elastomers such as ethylene-propylene-diene rubber (EPDM),[7−9] natural rubber (NR),[10−12] styrene-ethylene-butylene-styrene triblock copolymers (SEBSs),[9,13] polyolefin elastomers (POEs),[14] ethylene octane copolymers (EOCs),[15] and styrene-butadiene rubber (SBR).[16] TPEs based on PP and compatible nonpolar rubbers are widely studied, and attempts have been made to understand various aspects like morphology evolution,[7−11,13,14] mechanical properties,[7,10,11,13−16] dynamic mechanical properties,[7,11,13] rheological behavior,[7,8,12] thermal properties,[7,11,15] transparency[13] and percentage crystallinity[7,13] with reference to processing techniques[7] and blend ratios.[8−16]

In addition to the above studies, there are other studies in the literature that examine the preparation of PP-based TPEs by mixing PP with various incompatible polar elastomers like acrylic rubber (ACM),[17] acrylonitrile butadiene rubber (NBR),[18] recycled NBR (rNBR),[19] maleated ethylene propylene rubber (m-EPR),[20] and epichlorohydrin rubber (ECR).[21] It should be pointed out here that TPEs based on PP and polar elastomers do not display any useful properties due to poor compatibility between the blend components that arise from the large differences in polarity between the blend components (PP being nonpolar and elastomers being polar).[17−21] Therefore, a very low dosage (<10 wt %) of the third component known as a compatibilizer is added to compatibilize PP with polar elastomers, which in turn produces TPEs with useful properties.[17−21] Generally, incorporation of a compatibilizer into an incompatible polymer blend enhances the interfacial interaction/adhesion between the blend components by reducing the interfacial tension and leads to significantly improved physicomechanical properties.[17−22] In the literature, researchers have used various compatibilizers such as maleic anhydride-modified PP (MA-PP),[18,20,21] MA-PP/triethylene tetramine (TETA),[17] normal chlorinated polyethylene (n-CPE),[18] highly chlorinated polyethylene (h-CPE),[18] chlorinated polypropylene (CPP),[18] and epoxy resin (ER)[19] to prepare TPEs based on PP and various polar elastomers like ACM,[17] NBR,[18] rNBR,[19] m-EPR,[20] and ECR.[21] TPEs based on PP and various polar elastomers in the presence of appropriate compatibilizers have been found to show extraordinary properties like outstanding hot oil resistance, high heat resistance, high temperature resistance, superior flexibility, good weather resistance, excellent fatigue resistance, good abrasion resistance, and good low-temperature properties.[17−21]

Soares et al. have prepared TPEs based on PP and ACM (containing chlorine and carboxylic groups) with special reference to MA-PP in combination with TETA as a reactive compatibilizer.[17] It has been shown that the amino groups of TETA react with the anhydride groups of MA-PP to form imide groups, which in turn react with the chlorine and carboxylic groups of ACM rubber.[17] These reactions give rise to a network at the interface of PP/ACM blend, which in turn results in the significant increment of mechanical (maximum tensile strength, elongation at break value, tension set, and compression set) and dynamic mechanical properties.[17] Pan et al. have developed TPEs based on PP and NBR with four different kinds of compatibilizers such as n-CPE, h-CPE, CPP, and MA-PP.[18] It is seen that PP/NBR TPEs prepared using CPP as a compatibilizer shows better mechanical properties and oil resistance in comparison to PP/NBR TPEs prepared using n-CPE, h-CPE, and MA-PP as compatibilizers.[18] The significant enhancement in the oil resistance and mechanical properties (maximum tensile strength and elongation at break value) of PP/NBR blends in the presence of CPP has been attributed to the enhanced polar−polar interactions between the chlorine parts of CPP with the acrylonitrile parts of NBR.[18] Ismail et al. have studied the compatibilizing effect of ER on PP and rNBR based TPEs.[19] It has been shown that the compatibilizing effect of ER in the PP/rNBR blend has been attributed to the excellent chemical interactions between the epoxy parts of ER and the acrylonitrile parts of rNBR and is also due to the nonpolar physical interactions between ER and PP.[19] These reactions improve the interfacial interaction between PP and rNBR, which results in good mechanical properties (maximum tensile strength, elongation at break value, and Young's modulus).[19] Chatterjee and Naskar have found MA-PP as an effective compatibilizer for PP- and m-EPR-based TPEs.[20] They have reported that the compatibilized PP/m-EPR blend shows a higher crystallinity percentage value, good mechanical properties (maximum tensile strength, elongation at break value, tension set, hardness, and tear strength), and excellent recyclability due to the presence of polar−polar interactions between MA-PP and m-EPR.[20] In our recent publication, a unique TPE based on isotactic polypropylene (i-PP) and ECR has been prepared in the presence of MA-PP as the compatibilizer.[21] Fourier transform infrared (FTIR) spectroscopy has been used to understand the possible chemical interactions between i-PP and ECR in the presence of MA-PP as the compatibilizer.[21] It has been shown that the pendant maleic acid groups of MA-PP are capable of forming hydrogen bonds within the blend and also the anhydride portion of MA-PP interacts with the ECR and produces a saturated ester.[21] The enhanced interactions between i-PP and ECR in the presence of the MA-PP compatibilizer ultimately lead to a significant improvement in the overall properties.[21] Coran and Patel have prepared TPEs based on dimethylol phenolic-modified PP (DPM-PP) and NBR by technological compatibilization.[23] It has been shown that TPEs based on DPM-PP/NBR blends exhibit higher mechanical properties (stress at break, elongation at break, Young's modulus, and true stress at break) in comparison to the TPEs based on unmodified PP/NBR blends.[23] The formation of graft copolymers between DPM-PP and NBR leads to enhanced interfacial interaction between the blend components that in turn significantly improves the mechanical properties.[23]

The above studies clearly explain the crucial role of compatibilizers in improving the compatibility between PP and various polar elastomers for achieving enhanced properties.[17,18,21,22] Specifically, these compatibilizers have been found to reduce the interfacial tension between the blend components, enhance the interfacial interaction/adhesion

https://dx.doi.org/10.1021/acsomega.0c00423
ACS Omega 2020, 5, 12789−12808

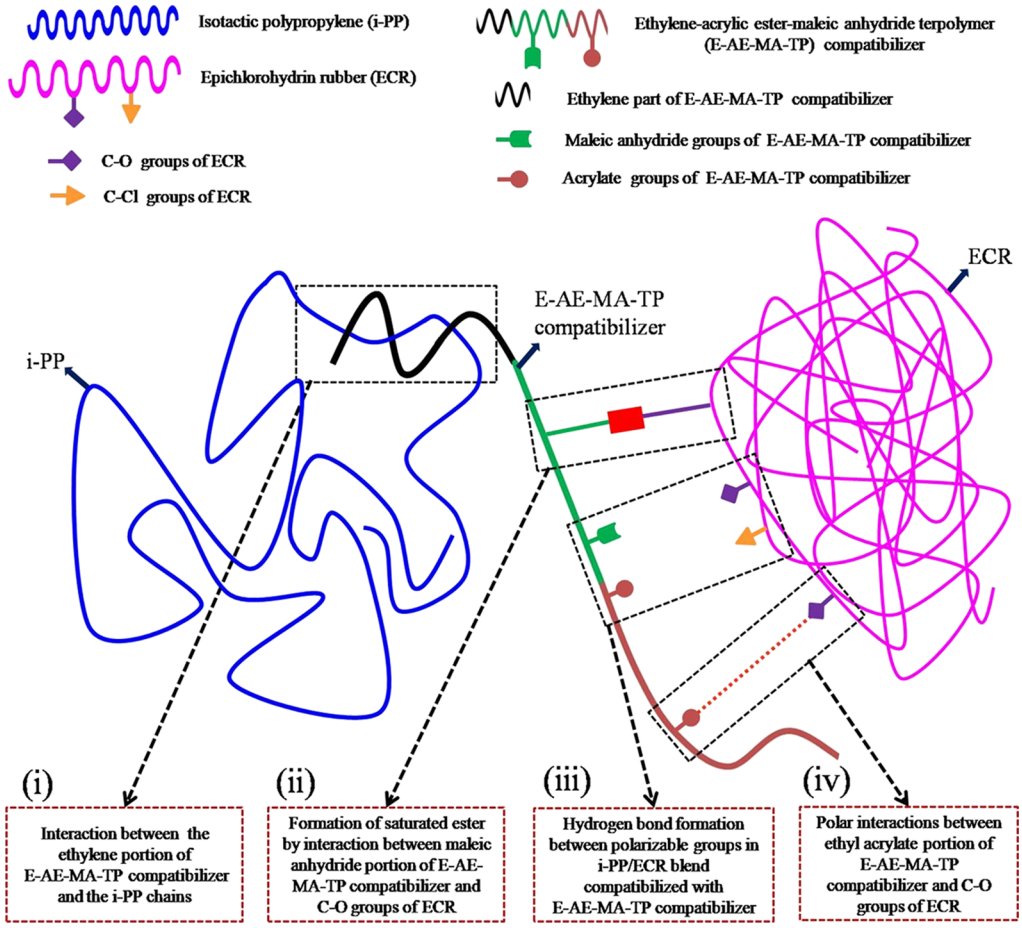

Figure 1. Schematic illustration showing the plausible multifaceted interactions of the E-AE-MA-TP compatibilizer with i-PP and ECR.

between the blend components, stabilize the blend morphology (against gross phase separation), and lead to a uniform/homogeneous dispersion of rubber domains in the PP matrix.[17,21,22] The compatibilizers used in the above studies have been found to have specific chemical interactions with both the PP phase and polar rubber phase.[17−22] Generally, one part of the compatibilizer reacts with the PP phase and the other part of the compatibilizer reacts with the polar rubber phase.[17−22] It is worth mentioning here that, till today, there have been no reports in the literature that examine the effect of a compatibilizer, which can have multifaceted interactions with the blend components (i.e., with PP and polar rubbers). Accordingly, in this work, attempts have been made to develop TPEs based on nonpolar i-PP and polar ECR in the presence of an ethylene-acrylic ester-maleic anhydride terpolymer (E-AE-MA-TP) as a compatibilizer. The E-AE-MA-TP compatibilizer is expected to establish multifaceted chemical interactions with i-PP and ECR in the following ways (Figure 1): (i) interaction between the ethylene portion of the E-AE-MA-TP compatibilizer and the i-PP chains, (ii) formation of a saturated ester by interaction between the maleic anhydride portion of the E-AE-MA-TP compatibilizer and the C−O groups of ECR, (iii) hydrogen bond formation between the polarizable groups in the i-PP/ECR blend compatibilized with the E-AE-MA-TP compatibilizer, and (iv) polar interactions between the ethyl acrylate portion of the E-AE-MA-TP compatibilizer and the C−O groups of ECR. The above plausible chemical interactions between i-PP and ECR in the presence of the E-AE-MA-TP compatibilizer can lead to the development of unique TPEs having good tensile strength and remarkably higher elongation. In the entire study, various analytical techniques such as contact angle measurements (surface energy studies), FTIR spectroscopy (analysis of the chemical interactions within the blend), universal testing machine (tensile stress−strain properties and tension set studies), modular compact rheometry (MCR) (rheological behavior and viscoelastic properties), differential scanning calorimetry (DSC) (melting and crystallization behavior), field emission scanning electron microscopy (FESEM), and atomic force microscopy (AFM) (morphological properties) have been employed to understand the effect of the E-AE-MA-TP compatibilizer in improving the overall properties of TPEs based on i-PP and ECR.

2. RESULTS AND DISCUSSION

2.1. Surface and Interface Property Studies. From eq 5, the graphs based on the plot between $\frac{\gamma_L(1+\cos\theta)}{2(\gamma_L^D)^{1/2}}$ and $\frac{(\gamma_L^P)^{1/2}}{(\gamma_L^D)^{1/2}}$ for $100_{i\text{-PP}}$, 100_{ECR}, and the E-AE-MA-TP compatibilizer are shown in Figure 2. The values of the polar and dispersion components of surface free energies obtained from the plots (for $100_{i\text{-PP}}$, 100_{ECR}, and E-AE-MA-TP compatibilizer) shown in Figure 2 are collected in Table 1.

The γ_S^P and γ_S^D values of $100_{i\text{-PP}}$ are 0.49 and 37.6 mN m^{-1}, respectively (Table 1). On the other hand, the γ_S^P and γ_S^D values of 100_{ECR} are 23.23 and 14.89 mN m^{-1}, respectively (Table 1). This confirms that there is a wide difference in polarity

https://dx.doi.org/10.1021/acsomega.0c00423
ACS Omega 2020, 5, 12789−12808

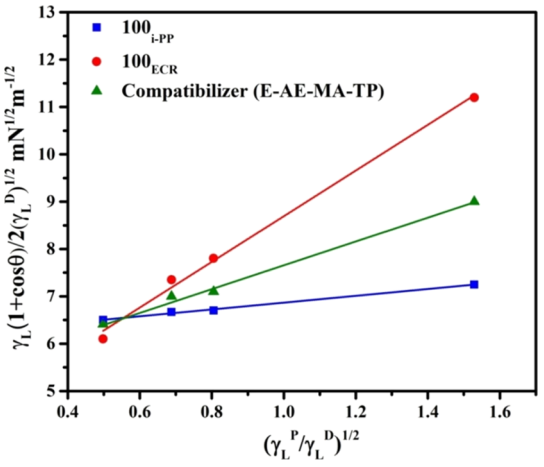

Figure 2. Plots based on eq 5 for contact angle liquids against $100_{i\text{-}PP}$, 100_{ECR}, and the E-AE-MA-TP compatibilizer.

between $100_{i\text{-}PP}$ and 100_{ECR}, which also suggests the poor compatibility between i-PP and ECR. From Table 1, it is also seen that the γ_S^P and γ_S^D values of the E-AE-MA-TP compatibilizer are 6.3 and 26.3 mN m^{-1}, respectively. The γ_S^P value of the E-AE-MA-TP compatibilizer is perhaps due to the presence of ethyl acrylate (29 wt %) and maleic anhydride (1.3 wt %) in the E-AE-MA-TP compatibilizer. On the other hand, the γ_S^D value of the E-AE-MA-TP compatibilizer is possibly due to the presence of ethylene (69.7 wt %) segments in the E-AE-MA-TP compatibilizer.

The interfacial tension values among i-PP/ECR, i-PP/E-AE-MA-TP, and ECR/E-AE-MA-TP have been calculated using eq 6 and the corresponding values are reported in Table 1. From Table 1, it is seen that the interfacial tension value between i-PP and ECR is 22.15 mN m^{-1}, which is very high and again confirms the poor compatibility between i-PP and ECR. On the other hand, the interfacial tension values between i-PP/E-AE-MA-TP and ECR/E-AE-MA-TP are 4.29 and 6.96 mN m^{-1}, respectively, which are relatively very low in comparison to the interfacial tension value between i-PP and ECR (Table 1). Also, the interfacial tension values between i-PP/E-AE-MA-TP and ECR/E-AE-MA-TP are close to each other. This validates the efficacy of the E-AE-MA-TP compatibilizer to interact with both the blend components (i-PP and ECR) as shown in Figure 1. Accordingly, it can be hypothesized that E-AE-MA-TP can act as an efficient compatibilizer for improving the compatibility between i-PP and ECR. The FTIR spectroscopy has been used to understand the chemical interactions between i-PP and ECR in the absence and presence of the E-AE-MA-TP compatibilizer. These results are discussed in the forthcoming section.

2.2. FTIR Analysis. Figure 3a depicts the FTIR spectra of 100_{ECR}, $100_{i\text{-}PP}$, and the E-AE-MA-TP compatibilizer. 100_{ECR} shows the following characteristic peaks at 746 cm^{-1} (corresponding to C−Cl stretching), 1100 cm^{-1} (corresponding to C−O stretching), 2867 cm^{-1} (corresponding to −CH− stretching), and 2914 cm^{-1} (corresponding to $-CH_2-$ symmetric stretching) (Table 2).[21] $100_{i\text{-}PP}$ represents the following characteristic peaks at 1375 cm^{-1} (corresponding to $-CH_3$ symmetric bending), 1458 cm^{-1} (corresponding to $-CH_3$ asymmetric bending), 2914 cm^{-1} (corresponding to $-CH_2-$ symmetric stretching), and 2950 cm^{-1} (corresponding to $-CH_3$ asymmetric stretching) (Table 2).[21,24] The E-AE-MA-TP compatibilizer represents the following characteristic peaks at 1156 and 1258 cm^{-1} (corresponding to C−O stretching of ethyl acrylate), 1467 cm^{-1} (corresponding $-CH_3$ asymmetric stretching of ethyl acrylate), and 1730 cm^{-1} (corresponding to C═O stretching of ethyl acrylate) (Table 2). In addition, the peak at 1782 cm^{-1} corresponds to the C═O stretching vibration of maleic anhydride present in the E-AE-MA-TP compatibilizer (Table 2). The FTIR spectra of $40_{i\text{-}PP}/60_{ECR}$ and $40_{i\text{-}PP}/60_{ECR}/5_C$ blends are shown in Figure 3b. The FTIR peaks and peak positions of the $40_{i\text{-}PP}/60_{ECR}$ blend remain unaltered with reference to the FTIR peaks and

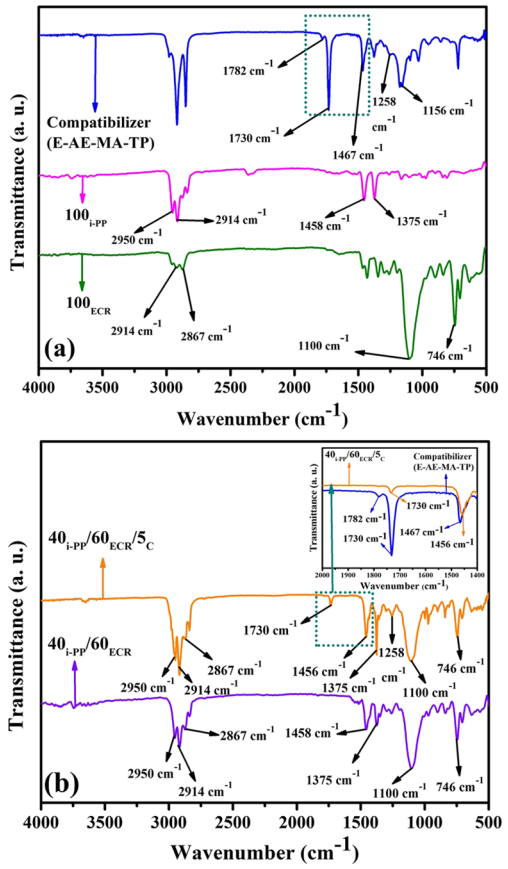

Figure 3. (a) FTIR spectra of 100_{ECR}, $100_{i\text{-}PP}$, and the E-AE-MA-TP compatibilizer and (b) FTIR spectra of the $40_{i\text{-}PP}/60_{ECR}$ blend and $40_{i\text{-}PP}/60_{ECR}/5_C$ blend. Inset of (b): FTIR spectra of the region between 2000 and 1400 cm^{-1} of the E-AE-MA-TP compatibilizer and $40_{i\text{-}PP}/60_{ECR}/5_C$ blend.

Table 1. Experimental Values of Polar (γ_S^P) and Dispersion (γ_S^D) Components of $100_{i\text{-}PP}$, 100_{ECR}, and the E-AE-MA-TP Compatibilizer

sl. no.	sample	γ_S^P (mN m^{-1})	γ_S^D (mN m^{-1})	γ_S (mN m^{-1})	interfacial tension γ_{12} (mN m^{-1})
1	$100_{i\text{-}PP}$	0.49	37.6	38.09	$\gamma_{i\text{-}PP/ECR}$ = 22.15
2	100_{ECR}	23.23	14.89	38.12	$\gamma_{i\text{-}PP/E\text{-}AE\text{-}MA\text{-}TP}$ = 4.29
3	compatibilizer (E-AE-MA-TP)	6.3	26.3	32.6	$\gamma_{ECR/E\text{-}AE\text{-}MA\text{-}TP}$ = 6.96

https://dx.doi.org/10.1021/acsomega.0c00423
ACS Omega 2020, 5, 12789−12808

Table 2. Peak Position and Their Assignment in the FTIR Spectra of 100_{ECR}, $100_{i\text{-}PP}$, E-AE-the MA-TP Compatibilizer, $40_{i\text{-}PP}/60_{ECR}$ Blend, and $40_{i\text{-}PP}/60_{ECR}/5_C$ Blend

	100_{ECR}		$100_{i\text{-}PP}$		compatibilizer (E-AE-MA-TP)		$40_{i\text{-}PP}/60_{ECR}$		$40_{i\text{-}PP}/60_{ECR}/5_C$	
sl. no.	peak at (cm^{-1})	peak assignments	peak at (cm^{-1})	peak assignments	peak at (cm^{-1})	peak assignments	peak at (cm^{-1})	peak assignments	peak at (cm^{-1})	peak assignments
1	746	C−Cl stretching	1375	$-CH_3$ symmetric bending	1156	C−O stretching	746	C−Cl stretching	746	C−Cl stretching
2	1100	C−O stretching	1458	$-CH_3$ asymmetric stretching	1258	C−O stretching	1100	C−O stretching	1100	C−O stretching
3	2867	−CH− stretching	2914	$-CH_2-$ symmetric stretching	1467	$-CH_3$ asymmetric stretching	1375	$-CH_3$ symmetric bending	1258	C−O stretching
4	2914	$-CH_2-$ symmetric stretching	2950	$-CH_3$ asymmetric stretching	1730	C═O stretching	1458	$-CH_3$ asymmetric stretching	1375	$-CH_3$ symmetric bending
5					1782	C═O stretching vibration of anhydride	2867	−CH− stretching	1456	$-CH_3$ asymmetric stretching
6							2914	$-CH_2-$ symmetric stretching	2867	−CH− stretching
7							2950	$-CH_3$ asymmetric stretching	2914	$-CH_2-$ symmetric stretching
8									2950	$-CH_3$ asymmetric stretching
9									1782	C═O stretching vibration of anhydride
10									1730	C═O stretching

Scheme 1. Scheme of the Possible Reaction between the Anhydride Part of the E-AE-MA-TP Compatibilizer and ECR

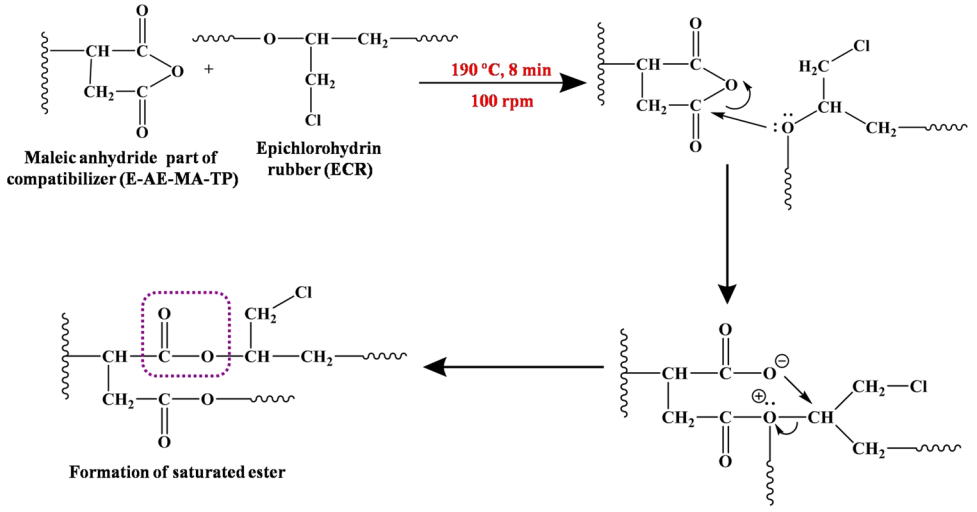

Scheme 2. Scheme of the Possible Reaction between Ethyl Acrylate Part of the E-AE-MA-TP Compatibilizer and ECR

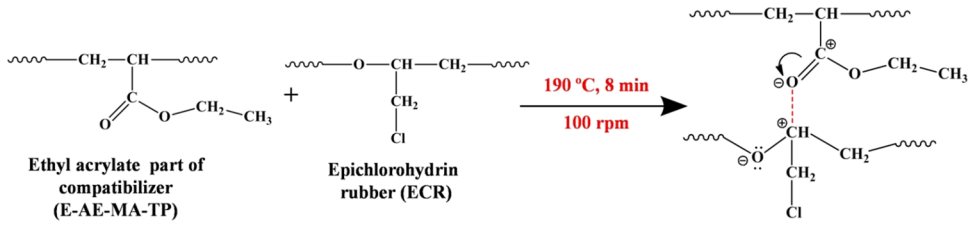

peak positions of $100_{i\text{-}PP}$ and 100_{ECR}, which ascertains that there exist no chemical reactions between i-PP and ECR in the absence of the E-AE-MA-TP compatibilizer (Table 2). Although there are no chemical reactions between i-PP and ECR in the absence of the E-AE-MA-TP compatibilizer, there could be some chemical interactions through secondary forces, which cannot be detected by FTIR spectroscopy.

The different types of plausible multifaceted interactions between the E-AE-MA-TP compatibilizer with i-PP and ECR are discussed below. First, the anhydride part of the E-AE-MA-TP compatibilizer can react with the C−O groups of ECR and form a saturated ester (around 1726 cm^{-1}) as shown in Scheme 1.

In our recent publication, it has been shown that a similar type of chemical interaction occurs between the anhydride part of the MA-PP compatibilizer and the C−O groups of ECR in i-PP/ECR-based TPEs.[21] However, here, the FTIR spectrum of the $40_{i\text{-}PP}/60_{ECR}/5_C$ blend does not explicitly show the presence of a saturated ester peak (around 1726 cm^{-1}), which is possibly due to the merging of the saturated ester peak

https://dx.doi.org/10.1021/acsomega.0c00423
ACS Omega 2020, 5, 12789−12808

Table 3. Mechanical Properties of $100_{i\text{-}PP}$ and i-PP/ECR Blends in the Absence and Presence of the E-AE-MA-TP Compatibilizer

sl. no.	sample code	ultimate tensile strength (MPa)	strain at break (%)	stress at 100% strain (MPa)	tension set (%)
1	$100_{i\text{-}PP}$	35.5 ± 1.5	14 ± 5		
2	$50_{i\text{-}PP}/50_{ECR}$	17.3 ± 1.5	31 ± 5		
3	$40_{i\text{-}PP}/60_{ECR}$	13.8 ± 1.0	46 ± 7		
4	$30_{i\text{-}PP}/70_{ECR}$	10.8 ± 1.0	62 ± 8		54 ± 1
5	$20_{i\text{-}PP}/80_{ECR}$	6.1 ± 0.5	96 ± 4		
6	$40_{i\text{-}PP}/60_{ECR}/3_C$	15.2 ± 1.0	270 ± 12	14.3 ± 1.0	
7	$40_{i\text{-}PP}/60_{ECR}/5_C$	17.2 ± 1.0	370 ± 12	15.4 ± 1.0	18 ± 1
8	$40_{i\text{-}PP}/60_{ECR}/7_C$	16.1 ± 1.0	310 ± 10	14.8 ± 1.0	
9	$30_{i\text{-}PP}/70_{ECR}/3_C$	13.2 ± 1.0	190 ± 12	12.8 ± 1.0	
10	$30_{i\text{-}PP}/70_{ECR}/5_C$	14.5 ± 1.0	270 ± 12	14.5 ± 1.0	20 ± 1
11	$30_{i\text{-}PP}/70_{ECR}/7_C$	13.8 ± 1.0	230 ± 10	13.2 ± 1.0	

(around 1726 cm^{-1}) with the ethyl acrylate peak (C═O stretching at 1730 cm^{-1}) of the E-AE-MA-TP compatibilizer. Second, the characteristic band at 1467 cm^{-1} (corresponding to the $-CH_3$ asymmetric stretching band of ethyl acrylate in the E-AE-MA-TP compatibilizer) shifts to 1456 cm^{-1} in the $40_{i\text{-}PP}/60_{ECR}/5_C$ blend (inset of Figure 3b), which is indicative of the interaction between the ethyl acrylate part of the E-AE-MA-TP compatibilizer and the ECR (Scheme 2).

Third, the carboxyl or carbonyl groups of maleic anhydride in the E-AE-MA-TP compatibilizer will form hydrogen bonds with the polar groups of ECR that can lead to efficient compatibilization. In the literature, Gaylord has reviewed the crucial role of hydrogen bonding between the carboxyl groups and carbonyl groups in the generation of toughened polyesters by melt mixing various acid- or anhydride-modified rubbers like maleic anhydride-grafted EPDM, poly(ethylene-*co*-isobutyl acrylate-*co*-methacrylic acid) ionomers, poly(ethylene-*co*-maleic acid-*co*-monomethyl maleate), and EPDM-*g*-fumaric acid with different thermoplastic polyesters such as poly(butylene terephthalate), poly(ethylene terephthalate), and polycarbonate (PC).[25] Gaylord has also reviewed the enhancement in the properties of polymer blends prepared by melt mixing of a maleic anhydride-grafted styrene-butadiene-styrene (S-B-S) triblock copolymer with thermoplastic polymers such as polyesters, polyurethanes, polyamide, PCs, polysulfones, polyacetals, polyphenylene sulfides, polyphenylene ethers, ionomers, nitrile polymers, vinyl alcohol copolymers, and vinyl ester copolymers.[25] It has been shown that the hydrogen bonding between the carbonyl/carboxyl groups of maleic anhydride in the S-B-S triblock copolymer and the polar groups in the thermoplastics undoubtedly plays a prominent role in developing compatible polymer blend systems with enhanced properties.[25] Benedetti et al. have shown that the blends based on diethyl maleate modified polyolefins (like ethylene propylene copolymer, PE, and atactic and isotactic PP) and poly(vinylchloride) (PVC) show good compatibility due to the hydrogen bonding interaction between the carbonyl groups in diethyl maleate-modified polyolefins and the tertiary hydrogen in PVC.[26] Based on the above discussions, here, it can be clearly ascertained that there are definite interactions existing between ECR and both the maleic anhydride and the acrylate parts of the E-AE-MA-TP compatibilizer (Schemes 1 and 2). In addition, it is worth mentioning here that the possibility of interaction between the ethylene portion of the E-AE-MA-TP compatibilizer and the i-PP chains should also be considered. Teh et al. have reviewed the compatibility between PE and PP and concluded that a very small amount of either PE in PP or PP in PE can generate PP/PE blends with enhanced properties (i.e., technologically compatible blends).[27] Here, since the compatibilizer content is relatively very low (5 wt %), there will not be any issues associated with the uniform mixing between the ethylene portion of the E-AE-MA-TP compatibilizer and the i-PP chains. FTIR studies clearly elucidate the presence of multiple point interactions in the $40_{i\text{-}PP}/60_{ECR}/5_C$ blend. On the contrary, FTIR studies confirm the absence of any type of interaction in the $40_{i\text{-}PP}/60_{ECR}$ blend. Accordingly, the i-PP/ECR blends compatibilized with the E-AE-MA-TP compatibilizer have been found to show better mechanical properties, rheological properties, melting/crystallization behavior, and morphological properties in comparison to i-PP/ECR blends without the compatibilizer. These results are discussed in detail in the subsequent sections.

2.3. Mechanical Property Studies. The mechanical properties of $100_{i\text{-}PP}$ and i-PP/ECR blends ($50_{i\text{-}PP}/50_{ECR}$, $40_{i\text{-}PP}/60_{ECR}$, $30_{i\text{-}PP}/70_{ECR}$, and $20_{i\text{-}PP}/80_{ECR}$) are listed in Table 3. The ultimate tensile strength values of all i-PP/ECR blends ($50_{i\text{-}PP}/50_{ECR}$, $40_{i\text{-}PP}/60_{ECR}$, $30_{i\text{-}PP}/70_{ECR}$, and $20_{i\text{-}PP}/80_{ECR}$) are lower in comparison to $100_{i\text{-}PP}$ (Table 3). The ultimate tensile strength continuously decreases with the increase in the concentrations of ECR in i-PP/ECR blends (Table 3).

This clearly confirms that increasing the concentration of ECR in i-PP/ECR blend leads to the reduction in the rigidity of the blends and accordingly the ultimate tensile strength value starts to decrease. On the other hand, the strain at break values of all i-PP/ECR blends ($50_{i\text{-}PP}/50_{ECR}$, $40_{i\text{-}PP}/60_{ECR}$, $30_{i\text{-}PP}/70_{ECR}$, and $20_{i\text{-}PP}/80_{ECR}$) are higher in comparison to $100_{i\text{-}PP}$ (Table 3). The strain at break continuously increases with the increase in the concentrations of ECR in i-PP/ECR blends. This shows that increasing the concentration of ECR in the i-PP/ECR blend reduces the stiffness of the blends and accordingly the strain at break value starts to increase. Reportedly, rubber/plastic blends are categorized as TPEs when they possess relatively good strain at break values (~100%).[6,21,28] It should be pointed here that none of these blends can be categorized as TPEs because they possess relatively very low strain at break values (<100%). This is attributed to the large polarity difference among the blend components as discussed earlier in the contact angle studies (Table 1). This wider difference in polarity between the blend components will lead to very low interfacial adhesion between i-PP and ECR and subsequently the stress transfer between the phases will be poor while stretching. The $50_{i\text{-}PP}/50_{ECR}$ blend shows a reasonably good ultimate tensile strength value with a

https://dx.doi.org/10.1021/acsomega.0c00423
ACS Omega 2020, 5, 12789−12808

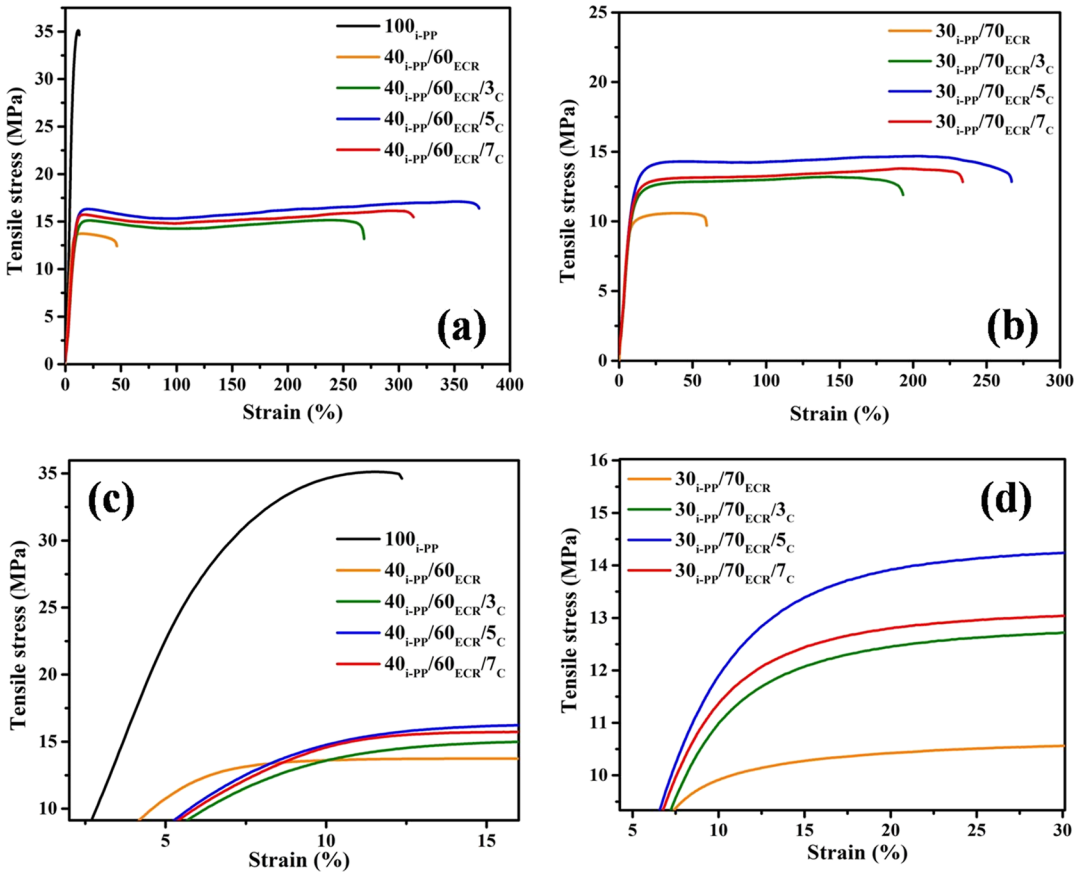

Figure 4. (a) Tensile stress versus strain curves of $100_{i\text{-}PP}$, the $40_{i\text{-}PP}/60_{ECR}$ blend, and $40_{i\text{-}PP}/60_{ECR}$ blend with different ratios (3, 5, and 7 wt %) of the E-AE-MA-TP compatibilizer, (b) tensile stress versus strain curves of the $30_{i\text{-}PP}/70_{ECR}$ blend and $30_{i\text{-}PP}/70_{ECR}$ blend with different ratios (3, 5, and 7 wt %) of the E-AE-MA-TP compatibilizer, (c) magnified tensile stress versus strain curves of $100_{i\text{-}PP}$, the $40_{i\text{-}PP}/60_{ECR}$ blend, and $40_{i\text{-}PP}/60_{ECR}$ blend with different ratios (3, 5, and 7 wt %) of the E-AE-MA-TP compatibilizer, and (d) magnified tensile stress versus strain curves of the $30_{i\text{-}PP}/70_{ECR}$ blend and $30_{i\text{-}PP}/70_{ECR}$ blend with different ratios (3, 5, and 7 wt %) of the E-AE-MA-TP compatibilizer.

very low strain at break value in comparison to the $40_{i\text{-}PP}/60_{ECR}$, $30_{i\text{-}PP}/70_{ECR}$, and $20_{i\text{-}PP}/80_{ECR}$ blends (Table 3). On the other hand, the $20_{i\text{-}PP}/80_{ECR}$ blend shows a reasonably good strain at break value with a very low ultimate tensile strength value in comparison to the $50_{i\text{-}PP}/50_{ECR}$, $40_{i\text{-}PP}/60_{ECR}$, and $30_{i\text{-}PP}/70_{ECR}$ blends (Table 3). Accordingly, $50_{i\text{-}PP}/50_{ECR}$ and $20_{i\text{-}PP}/80_{ECR}$ blends are not taken for further investigations. It is interesting to note that $40_{i\text{-}PP}/60_{ECR}$ and $30_{i\text{-}PP}/70_{ECR}$ blends show optimal properties (with respect to ultimate tensile strength and strain at break values) in comparison to $50_{i\text{-}PP}/50_{ECR}$ and $20_{i\text{-}PP}/80_{ECR}$ blends (Table 3). Therefore, $40_{i\text{-}PP}/60_{ECR}$ and $30_{i\text{-}PP}/70_{ECR}$ blends are taken for detailed investigations by adding different ratios of the E-AE-MA-TP compatibilizer. Table 3 represents the effect of ratio of E-AE-MA-TP compatibilizer on the mechanical properties of $40_{i\text{-}PP}/60_{ECR}$ and $30_{i\text{-}PP}/70_{ECR}$ blends.

Figure 4a,b compares the tensile stress−strain plots of $40_{i\text{-}PP}/60_{ECR}$ and $30_{i\text{-}PP}/70_{ECR}$ blends with different ratios of the E-AE-MA-TP compatibilizer. It is observed that the mechanical properties (ultimate tensile strength, strain at break, and stress at 100% strain values) of the blends ($40_{i\text{-}PP}/60_{ECR}$ and $30_{i\text{-}PP}/70_{ECR}$) increase when the concentration of the E-AE-MA-TP compatibilizer is increased from 3 to 5 wt %. However, the mechanical properties (ultimate tensile strength, strain at break, and stress at 100% strain values) of the blends ($40_{i\text{-}PP}/60_{ECR}$ and $30_{i\text{-}PP}/70_{ECR}$) start to decrease at a higher concentration (7 wt %) of the E-AE-MA-TP compatibilizer (Figure 4a,b and Table 3).

The ultimate tensile strength value and strain at break value of the $40_{i\text{-}PP}/60_{ECR}/5_C$ blend is around 24 and 704%, respectively, higher in comparison to $40_{i\text{-}PP}/60_{ECR}$ blend (Table 3). On the other hand, the ultimate tensile strength value and strain at break value of the $30_{i\text{-}PP}/70_{ECR}/5_C$ blend is around 34 and 346%, respectively, higher in comparison to the $30_{i\text{-}PP}/70_{ECR}$ blend (Table 3). The incorporation of the E-AE-MA-TP compatibilizer significantly increases the interfacial adhesion/interaction between i-PP and ECR, which will lead to efficient transfer of stress from the continuous phase (i-PP phase) to the dispersed phase (ECR phase) through the interface. Accordingly, the dispersed ECR phase will be able to undertake more stress and lead to higher strain at break values and ultimate tensile strength values (Table 3). The contact angle studies and the FTIR studies discussed in the previous sections provide evidence for the strong chemical interactions/interfacial adhesion between i-PP and ECR in the presence of the E-AE-MA-TP compatibilizer. The morphological studies by FESEM and AFM also provide clear evidence for the remarkable reduction in the particle size of the dispersed ECR phase in the i-PP matrix after incorporation of the E-AE-MA-TP as compatibilizer. This again confirms the enhanced interfacial adhesion between i-PP and ECR in the presence of E-AE-MA-TP as the compatibilizer. The morphological studies

https://dx.doi.org/10.1021/acsomega.0c00423
ACS Omega 2020, 5, 12789−12808

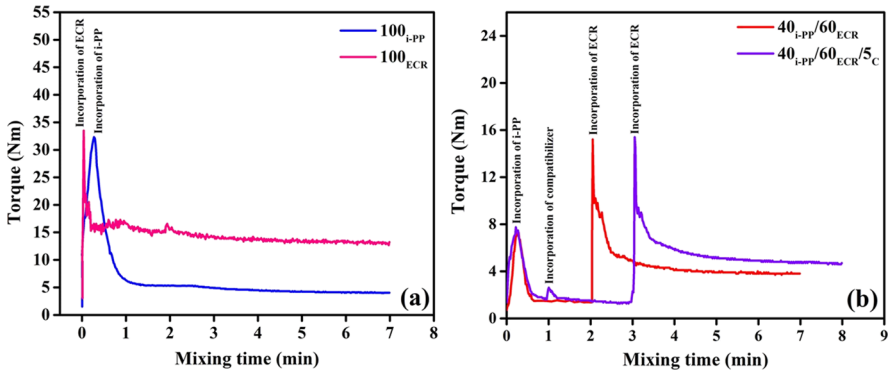

Figure 5. Mixing time versus torque curves (at rotor speed of 100 rpm and at 190 °C) of (a) $100_{i\text{-}PP}$ and 100_{ECR} and the (b) $40_{i\text{-}PP}/60_{ECR}$ blend and $40_{i\text{-}PP}/60_{ECR}/5_C$ blend.

of $40_{i\text{-}PP}/60_{ECR}$ and $40_{i\text{-}PP}/60_{ECR}/5_C$ blends are discussed in detail in the later section.

In the literature, Setua et al. have shown that TPEs based on high-density polyethylene (HDPE) and NBR show very low mechanical properties due to the poor compatibility between the blend components.[28] In the same work, Setua et al. have also shown that TPEs based on phenolic resin-modified HDPE (Ph-HDPE) and NBR show improved mechanical properties. This is due to the enhanced interaction of the Ph-HDPE with NBR through formation of a graft copolymer, which in turn increases the interfacial adhesion and subsequently improves the mechanical properties.[28] In another work, George et al. have shown that the TPEs based on PP and NBR show very low mechanical properties due to the poor compatibility between the blend components.[29] In the same work, George et al. have shown that the incorporation of either MA-PP or phenolic-modified PP (Ph-PP) as the compatibilizer in the PP/NBR blend leads to the dipolar interaction between MA-PP and NBR or formation of graft copolymers between Ph-PP and NBR, respectively, which in turn leads to enhanced interfacial adhesion and subsequently improves the mechanical properties.[29] Regarding the yielding point in tensile stress−strain curves, $100_{i\text{-}PP}$ has been found to show a semiductile behavior with an unstable post-yield deformation (Figure 4c). Accordingly, the tensile bar of $100_{i\text{-}PP}$ failed by localized yielding without formation of a necking zone (Figure 4c). In addition, noncompatibilized i-PP/ECR blends and compatibilized i-PP/ECR blends also do not show any clear yield point (Figure 4c,d). In the literature, there are a few other TPEs based on PP/EPDM blends[30] and PP/NR blends,[31] which also does not show any clear yield point in the tensile stress−strain curves.

The tension set value of the $30_{i\text{-}PP}/70_{ECR}$ and $30_{i\text{-}PP}/70_{ECR}/5_C$ blends have been found to be 54% and 20% respectively (Table 3). The $40_{i\text{-}PP}/60_{ECR}$ blend does not show tension set value at 50% strain because the sample failed below 50% strain (Table 3). On the contrary, the tension set value of the $40_{i\text{-}PP}/60_{ECR}/5_C$ blend has been found to be 18% (Table 3). It is clear that the presence of E-AE-MA-TP compatibilizer has significantly improved the elastic recovery behavior of $40_{i\text{-}PP}/60_{ECR}$ blend and $30_{i\text{-}PP}/70_{ECR}$ blend after prolonged extension, which is a typical requirement of a TPE.[6,21,28] The efficacy of the E-AE-MA-TP compatibilizer to interact with both the blend components (i-PP and ECR) significantly enhances the interfacial adhesion (by reducing the interfacial tension) between the phases, which in turn leads to better elastic recovery behavior (low tension set values). In the literature, it has been shown that the addition of various compatibilizers like MA-PP/TETA,[17] MA-PP or Ph-PP,[32] and Ph-PE or MA-HDPE[33] to different polymer blends such as PP/ACM,[17] PP/epoxidized NR,[32] and HDPE/maleated NR[33] enhances the interfacial adhesion (by reducing the interfacial tension) between the blend components, which in turn leads to low tension set values.

It should be pointed here that the ultimate tensile strength and strain at break value of $40_{i\text{-}PP}/60_{ECR}/5_C$ blend is around 18 and 37% higher in comparison to the $30_{i\text{-}PP}/70_{ECR}/5_C$ blend (Table 3). Also, the $40_{i\text{-}PP}/60_{ECR}/5_C$ blend shows better elastic recovery behavior when compared to the $30_{i\text{-}PP}/70_{ECR}/5_C$ blend (Table 3). The above results indicate that the effect of the E-AE-MA-TP compatibilizer is more prominent in the $40_{i\text{-}PP}/60_{ECR}$ blend in comparison to the $30_{i\text{-}PP}/70_{ECR}$ blend. Accordingly, $40_{i\text{-}PP}/60_{ECR}$ and $40_{i\text{-}PP}/60_{ECR}/5_C$ blends are selected for detailed investigations.

2.4. Mixing Torque Analysis. The Haake Rheocord used in this study (for the preparation of samples) is an internal mixer that has various mixing elements such as rotors, rotor shafts, ram, thermocouples, etc. The shaft of the rotors experiences different torque values based on the viscosity of the mixture, and this torque is the measure of viscosity. Here, the variation of mixing torque with respect to time has been analyzed to get a better idea regarding the extent of interaction between i-PP and ECR in the absence and presence of the E-AE-MA-TP compatibilizer. Figure 5a shows the mixing torque profiles of $100_{i\text{-}PP}$ and 100_{ECR}. The kinks seen in the mixing torque profiles of $100_{i\text{-}PP}$ and 100_{ECR} arise when i-PP or ECR is incorporated into the mixing chamber of the internal mixer (Figure 5a). It is seen that $100_{i\text{-}PP}$ and 100_{ECR} achieve an equilibrium mixing torque at around 3 min (Figure 5a). The equilibrium mixing torque (after 3 min of mixing) of 100_{ECR} is higher than that of $100_{i\text{-}PP}$ (Figure 5a). This is due to the higher melt viscosity of ECR in comparison to i-PP under specified mixing conditions.

The mixing torque profiles of $40_{i\text{-}PP}/60_{ECR}$ and $40_{i\text{-}PP}/60_{ECR}/5_C$ blends are compared in Figure 5b. The kinks seen in the mixing torque profiles of the $40_{i\text{-}PP}/60_{ECR}$ blend arise when i-PP and ECR are added into the internal mixing chamber (Figure 5b). The kinks seen in the mixing torque profiles of the $40_{i\text{-}PP}/60_{ECR}/5_C$ blend arise when i-PP, ECR, and the E-AE-MA-TP compatibilizer are added into the internal mixing chamber (Figure 5b). From Figure 5b, it is seen that the equilibrium mixing torque (after 5 min) of the $40_{i\text{-}PP}/60_{ECR}/5_C$ blend is higher in comparison to the $40_{i\text{-}PP}/60_{ECR}$ blend. This shows the higher melt viscosity of the $40_{i\text{-}PP}/60_{ECR}/5_C$ blend as

https://dx.doi.org/10.1021/acsomega.0c00423
ACS Omega 2020, 5, 12789−12808

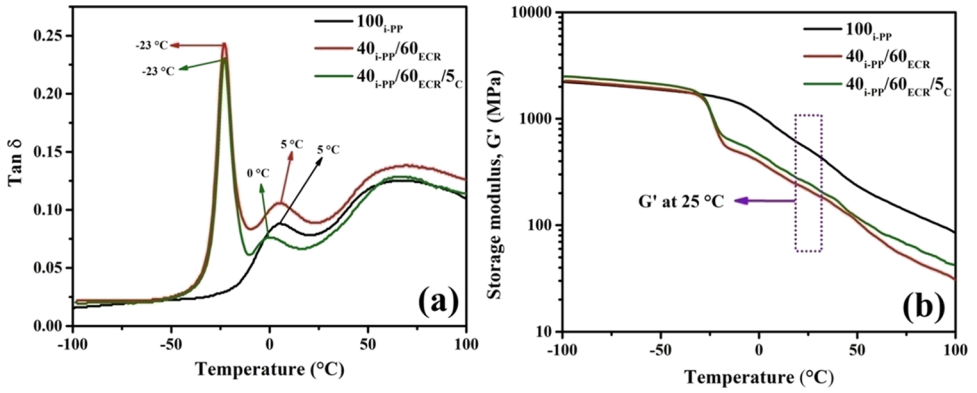

Figure 6. (a) Tan δ versus temperature curves of $100_{i\text{-PP}}$, the $40_{i\text{-PP}}/60_{ECR}$ blend, and $40_{i\text{-PP}}/60_{ECR}/5_C$ blend and (b) storage modulus (G') versus temperature curves of $100_{i\text{-PP}}$, the $40_{i\text{-PP}}/60_{ECR}$ blend, and $40_{i\text{-PP}}/60_{ECR}/5_C$ blend.

Table 4. T_g, tan δ Peak Height, and Storage Modulus (G') Values for $100_{i\text{-PP}}$, $40_{i\text{-PP}}/60_{ECR}$ Blend, and $40_{i\text{-PP}}/60_{ECR}/5_C$ Blend

		tan δ peak for ECR		tan δ peak for i-PP		
sl. no.	sample code	T_g (°C)	tan δ peak height	T_g (°C)	tan δ peak height	storage modulus at 25 °C (MPa)
1	$100_{i\text{-PP}}$			5 ± 1.0	0.08 ± 0.01	510 ± 4
2	$40_{i\text{-PP}}/60_{ECR}$	−23 ± 0.5	0.24 ± 0.02	5 ± 1.0	0.11 ± 0.02	214 ± 5
3	$40_{i\text{-PP}}/60_{ECR}/5_C$	−23 ± 0.5	0.22 ± 0.01	0	0.07 ± 0.01	247 ± 3

compared to the $40_{i\text{-PP}}/60_{ECR}$ blend, which is attributed to the enhanced interfacial interaction between i-PP and ECR in the presence of the E-AE-MA-TP compatibilizer. Such an enhancement in the blend viscosity by addition of the compatibilizer has been reported by several authors for various blends such as PP/ACM blends compatibilized with MA-PP/TETA,[17] PP/NBR blends compatibilized with either an MA-PP/amino compound or glycidyl methacrylate-grafted PP (GMA-PP) or a GMA-PP/amino compound[34] and polystyrene/NBR blends compatibilized with a styrene acrylonitrile copolymer.[35] It has been shown that the compatibilizers have been found to enhance the interfacial interactions between the blend components and lead to higher blend viscosity.[17,34,35] Here, the mixing torque analysis clearly shows the higher melt viscosity of the $40_{i\text{-PP}}/60_{ECR}/5_C$ blend in comparison to the $40_{i\text{-PP}}/60_{ECR}$ blend due to the presence of strong interactions between i-PP and ECR in the presence of the E-AE-MA-TP compatibilizer. This corroborates well with the contact angle studies and FTIR studies regarding the enhancement in the interfacial adhesion/interaction (reduction in the interfacial tension) between i-PP and ECR in the presence of the E-AE-MA-TP compatibilizer. The rheological studies (frequency sweep studies) also provide firm evidence for the presence of strong interactions between i-PP and ECR in the presence of the E-AE-MA-TP compatibilizer. These results are discussed in detail in the forthcoming section.

2.5. Rheological Property Studies. *2.5.1. Viscoelasticity Studies.* The tan δ versus temperature plots of $100_{i\text{-PP}}$ and i-PP/ECR blends ($40_{i\text{-PP}}/60_{ECR}$ and $40_{i\text{-PP}}/60_{ECR}/5_C$) are shown in Figure 6a. The viscoelastic properties of $100_{i\text{-PP}}$ and i-PP/ECR blends ($40_{i\text{-PP}}/60_{ECR}$ and $40_{i\text{-PP}}/60_{ECR}/5_C$) are compared in Table 4.

Generally, the tan δ peak temperature in tan δ versus temperature plot is considered as the T_g of the polymer.[22,36] Here, the tan δ peak temperature of i-PP occurring at 5 °C (β transition) corresponds to the glass transition temperature of i-PP, where glass to rubber relaxation of amorphous portions of i-PP takes place (Table 4).[13,37] The $40_{i\text{-PP}}/60_{ECR}$ blend shows two distinct tan δ peaks at −23 and 5 °C that exactly correspond to the T_g values of ECR and i-PP, respectively, which confirms the incompatibility between i-PP and ECR (Figure 6a). In the literature, various incompatible polymer blends such as nylon/EPDM rubber,[36] HDPE/ethylene vinyl acetate (EVA)[38] copolymers, and i-PP/NBR[22] have been found to show two distinct T_g values (corresponding to the T_g of their individual blend components) in their respective tan δ versus temperature plots, which has been taken as a sign of the incompatibility between the blend components. The $40_{i\text{-PP}}/60_{ECR}/5_C$ blend shows tan δ peaks at −23 and 0 °C that correspond to the T_g values of ECR and i-PP, respectively (Figure 6a). The T_g values of ECR in the $40_{i\text{-PP}}/60_{ECR}$ blend and $40_{i\text{-PP}}/60_{ECR}/5_C$ blend occurs at −23 °C (Table 4). On the other hand, the T_g values of i-PP in the $40_{i\text{-PP}}/60_{ECR}$ blend and $40_{i\text{-PP}}/60_{ECR}/5_C$ blend occur at 5 and 0 °C, respectively (Table 4). Therefore, it is clear that incorporation of 5 wt % E-AE-MA-TP compatibilizer to the $40_{i\text{-PP}}/60_{ECR}$ blend does not alter the T_g of ECR. However, incorporation of 5 wt % E-AE-MA-TP compatibilizer to the $40_{i\text{-PP}}/60_{ECR}$ blend shifts the T_g of i-PP to a lower temperature (toward T_g of ECR), which indicates the enhanced interaction between i-PP and ECR in the presence of the E-AE-MA-TP compatibilizer. In the literature, Komalan et al. have shown that addition of ethylene propylene monomer-grafted maleic anhydride (EPM-g-MA) as a compatibilizer to incompatible nylon/EPDM blend results in the shifting of the T_g of nylon to a lower temperature.[36] This has been attributed to the enhanced interaction (interactions between amine groups and maleic anhydride groups of nylon and EPM-g-MA respectively) between nylon and EPDM in the presence of EPM-g-MA as the compatibilizer.[36] In another work, John et al. have shown that addition of maleic-modified PE (MA-PE) as a compatibilizer to the incompatible HDPE/EVA blend results in the shifting of the T_g of HDPE to a lower temperature.[38] This has been attributed to the enhanced interaction (interactions between maleic anhydride groups and vinyl acetate groups of MA-PE and EVA, respectively) between HDPE and EVA in the presence of MA-PE as the

https://dx.doi.org/10.1021/acsomega.0c00423
ACS Omega 2020, 5, 12789−12808

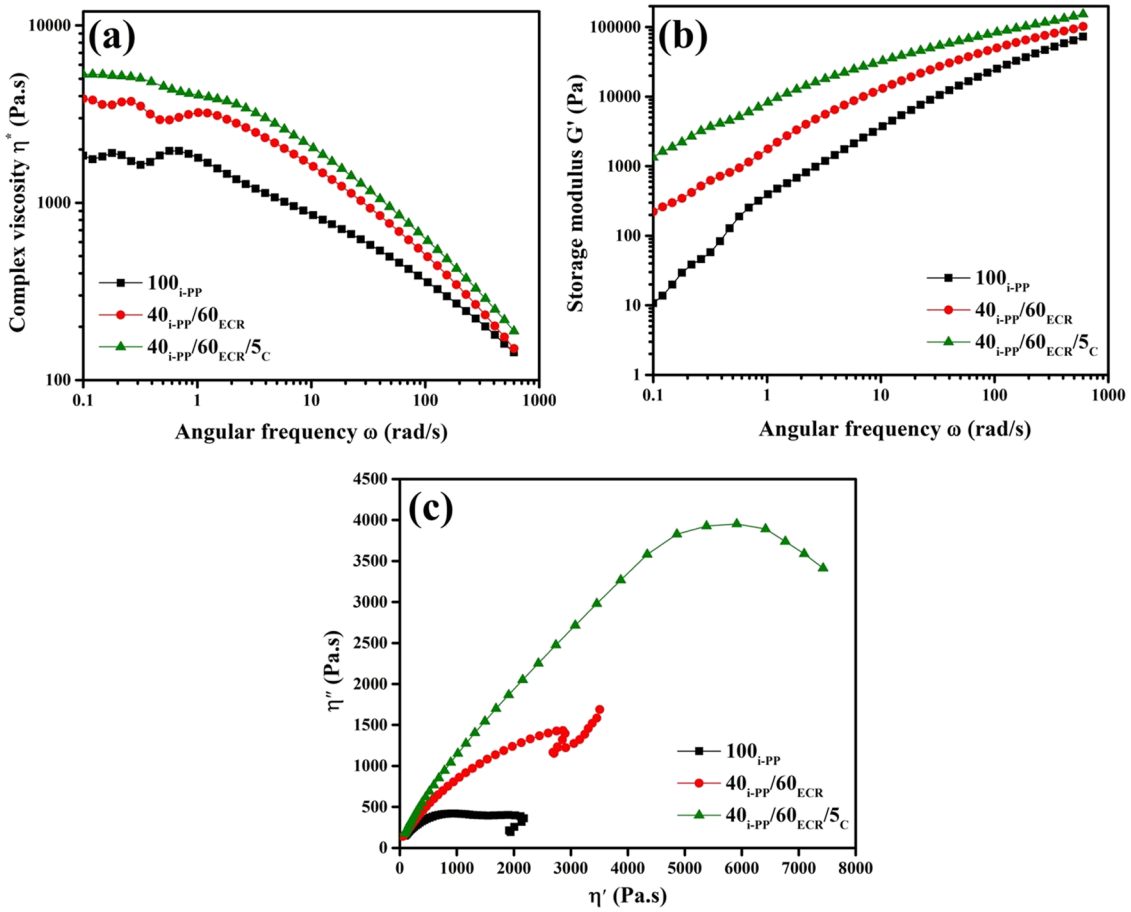

Figure 7. (a) Complex viscosity versus angular frequency plots for $100_{i\text{-PP}}$, the $40_{i\text{-PP}}/60_{ECR}$ blend, and $40_{i\text{-PP}}/60_{ECR}/5_C$ blend, (b) storage modulus versus angular frequency plots for $100_{i\text{-PP}}$, the $40_{i\text{-PP}}/60_{ECR}$ blend, and $40_{i\text{-PP}}/60_{ECR}/5_C$ blend, and (c) Cole−Cole plots for $100_{i\text{-PP}}$, the $40_{i\text{-PP}}/60_{ECR}$ blend, and $40_{i\text{-PP}}/60_{ECR}/5_C$ blend.

compatibilizer.[38] The tan δ peak height values corresponding to ECR and i-PP of the $40_{i\text{-PP}}/60_{ECR}/5_C$ blend is lower when compared to the tan δ peak height values corresponding to ECR and i-PP of the $40_{i\text{-PP}}/60_{ECR}$ blend (Figure 6a and Table 4). This suggests the existence of restriction in chain mobility in the $40_{i\text{-PP}}/60_{ECR}/5_C$ blend due to the presence of the E-AE-MA-TP compatibilizer. This observation is in line with the results reported in the literature for PP/ECR blends compatibilized with MA-PP[21] and PP/NBR blends compatibilized with either an MA-PP/amino compound or a GMA-PP or GMA-PP/amino compound.[34] The storage modulus (G') versus temperature plots of $100_{i\text{-PP}}$ and i-PP/ECR blends ($40_{i\text{-PP}}/60_{ECR}$ and $40_{i\text{-PP}}/60_{ECR}/5_C$) are shown in Figure 6b. The storage modulus values (at 25 °C) of $100_{i\text{-PP}}$ and i-PP/ECR blends ($40_{i\text{-PP}}/60_{ECR}$ and $40_{i\text{-PP}}/60_{ECR}/5_C$) are shown in Table 4. It is observed that the storage modulus value (at 25 °C) of the $40_{i\text{-PP}}/60_{ECR}/5_C$ blend is higher in comparison to that of the $40_{i\text{-PP}}/60_{ECR}$ blend (Figure 6b and Table 4). This clearly indicates the presence of an enhanced interfacial interaction between i-PP and ECR in the $40_{i\text{-PP}}/60_{ECR}/5_C$ blend due to the presence of the E-AE-MA-TP compatibilizer. It is worth mentioning here that the ultimate tensile strength of the $40_{i\text{-PP}}/60_{ECR}/5_C$ blend (17.2 MPa) is reasonably higher when compared to the $40_{i\text{-PP}}/60_{ECR}$ blend (13.8 MPa) (Table 3). On the other hand, the storage modulus value (at 25 °C) of the $40_{i\text{-PP}}/60_{ECR}/5_C$ blend (247 MPa) is significantly higher in comparison to that of the $40_{i\text{-PP}}/60_{ECR}$ blend (214 MPa) (Table 4). This suggests that the role of the E-AE-MA-TP compatibilizer in improving the storage modulus (at 25 °C) of the i-PP/ECR blend is more prominent in comparison to the role of the E-AE-MA-TP compatibilizer in improving the ultimate tensile strength of the i-PP/ECR blend. In the literature, various polymer blends like PP/ACM blends compatibilized with MA-PP/TETA,[17] PP/ECR blends compatibilized with MA-PP,[21] and PP/NBR blends compatibilized with either an MA-PP/amino compound or a GMA-PP or GMA-PP/amino compound[34] have been found to show higher storage modulus values in comparison to their respective non compatibilized polymer blends. This has been ascribed to the presence of enhanced interfacial interactions in the compatibilized polymer blends due to the presence of the compatibilizer, which in turn increases the storage modulus values.[17,21,34]

2.5.2. Frequency Sweep Studies. The complex viscosity (η^*) versus angular frequency (ω) plots and storage modulus (G') versus angular frequency (ω) plots of $100_{i\text{-PP}}$ and i-PP/ECR blends ($40_{i\text{-PP}}/60_{ECR}$ and $40_{i\text{-PP}}/60_{ECR}/5_C$) are shown in Figure 7ab, respectively.

From Figure 7a, it is seen that the complex viscosity of $100_{i\text{-PP}}$, the $40_{i\text{-PP}}/60_{ECR}$ blend, and $40_{i\text{-PP}}/60_{ECR}/5_C$ blend decreases with an increase in the frequency. On the other hand, from Figure 7b, it is seen that the storage modulus of $100_{i\text{-PP}}$, the $40_{i\text{-PP}}/60_{ECR}$ blend, and $40_{i\text{-PP}}/60_{ECR}/5_C$ blend increases with an increase in the frequency. It should be

https://dx.doi.org/10.1021/acsomega.0c00423
ACS Omega 2020, 5, 12789−12808

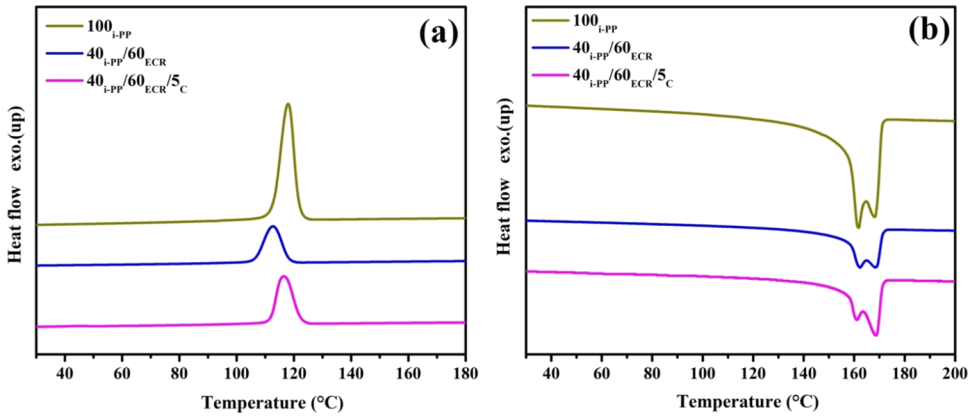

Figure 8. (a) Crystallization curves of $100_{i\text{-PP}}$, the $40_{i\text{-PP}}/60_{ECR}$ blend, and $40_{i\text{-PP}}/60_{ECR}/5_C$ blend and (b) melting curves of $100_{i\text{-PP}}$, the $40_{i\text{-PP}}/60_{ECR}$ blend, and $40_{i\text{-PP}}/60_{ECR}/5_C$ blend.

Table 5. Crystallization and Melting Parameters for $100_{i\text{-PP}}$, the $40_{i\text{-PP}}/60_{ECR}$ Blend, and $40_{i\ PP}/60_{ECR}/5_C$ Blend

		cooling			2nd melting			
		crystallization onset temperature	crystallization peak temperature	heat of crystallization	lower melting temperature	higher melting temperature	melting enthalpy	degree of crystallinity
sl. no.	sample	T_{OC} (°C)	T_{PC} (°C)	ΔH_C (J g^{-1})	T_{LM} (°C)	T_{HM} (°C)	ΔH_M (J g^{-1})	(X_C (%))
1	$100_{i\text{-PP}}$	122 ± 0.3	118 ± 0.2	98.9 ± 1.4	161 ± 0.4	168 ± 0.1	89.1 ± 4.7	42.6 ± 2.3
2	$40_{i\text{-PP}}/60_{ECR}$	117 ± 0.3	112 ± 0.4	27.2 ± 1.0	161 ± 0.2	168 ± 0.3	31.1 ± 0.6	37.2 ± 0.7
3	$40_{i\text{-PP}}/60_{ECR}/5_C$	122 ± 0.6	116 ± 0.1	38.1 ± 0.5	161 ± 0.3	168 ± 0.4	39.6 ± 0.7	42.1 ± 0.7

pointed out here that, in the entire frequency range, the $40_{i\text{-PP}}/60_{ECR}/5_C$ blend shows higher complex viscosity values and storage modulus values in comparison to the $40_{i\text{-PP}}/60_{ECR}$ blend due to the enhanced interfacial interaction between i-PP and ECR in the presence of the E-AE-MA-TP compatibilizer. The results obtained from the frequency sweep studies are in accord with the earlier results of mixing torque analysis (melt viscosity) and temperature sweep studies (storage modulus values). In the literature, Codou et al. have shown that a PP/nylon 6/poly(lactic acid) (PLA) blend in the presence of MA-PP as the compatibilizer shows higher complex viscosity values and storage modulus values (across the full range of frequency) in comparison to a PP/nylon 6/PLA blend having no compatibilizer.[39] This has been ascribed to the enhanced chemical interactions (interactions between amine groups, carboxylic groups, and maleic anhydride groups of nylon 6, PLA, and MA-PP, respectively) among PP, nylon 6, and PLA in the presence of MA-PP as the compatibilizer.[39] In another work, Zanjanijam et al. have shown that a PP/poly(vinyl butyral) (PVB) blend in the presence of MA-PP as the compatibilizer shows higher complex viscosity values and storage modulus values (across the full range of frequency) in comparison to PP/PVB having no compatibilizer.[40] This has been attributed to the enhanced chemical interactions (interactions between hydroxyl groups and maleic anhydride groups of PVB and MA-PP, respectively) between PP and PVB in the presence of MA-PP as the compatibilizer.[40]

Cole−Cole plots are widely used to understand the structure of polymers and polymer blends.[39,40] It is also well known that the plot between the imaginary viscosity (η'') and real viscosity (η') in a Cole−Cole plot gives information about the compatibility in polymer blends.[39,40] Generally, when a polymer blend is compatible, the corresponding Cole−Cole plot will show a perfect semicircular arc/curve.[39,40] On the other hand, if the polymer blend is incompatible, the corresponding Cole−Cole plot will show a modified semicircular arc/curve.[39,40] Here, Cole−Cole plots have been constructed by plotting the imaginary viscosity (η'') against the real viscosity (η') for $100_{i\text{-PP}}$ and i-PP/ECR blends ($40_{i\text{-PP}}/60_{ECR}$ and $40_{i\text{-PP}}/60_{ECR}/5_C$) at 190 °C. The Cole−Cole plot of $100_{i\text{-PP}}$ shows a single semicircular arc due to the homogeneous composition (Figure 7c). The Cole−Cole plot of the $40_{i\text{-PP}}/60_{ECR}$ blend does not show a perfect semicircular curve, and there is also a shoulder in the right-hand side of the plot (Figure 7c). FTIR studies and contact angle studies of the $40_{i\text{-PP}}/60_{ECR}$ blend (discussed earlier) confirmed the absence of any type of interaction between i-PP and ECR, which in turn leads to the development of an inhomogeneous and incompatible polymer blend. Accordingly, the Cole−Cole plot of the $40_{i\text{-PP}}/60_{ECR}$ blend does not show a perfect semicircular curve. On the other hand, the Cole−Cole plot of the $40_{i\text{-PP}}/60_{ECR}/5_C$ blend shows a perfect semicircular curve (Figure 7c). FTIR studies and contact angle studies of the $40_{i\text{-PP}}/60_{ECR}/5_C$ blend (discussed earlier) endorsed the efficacy of the E-AE-MA-TP compatibilizer in significantly enhancing the interaction between i-PP and ECR, which in turn leads to the development of a more uniform and homogeneous polymer blend. Accordingly, the Cole−Cole plot of the $40_{i\text{-PP}}/60_{ECR}/5_C$ blend shows a perfect semicircular curve. In the literature, the Cole−Cole plots (η'' vs η') of the PP/nylon 6/PLA blend compatibilized with MA-PP[39] and the PP/PVB blend compatibilized with MA-PP[40] show a perfect semicircular curve in comparison to those of their respective non-compatibilized polymer blends. This has been attributed to the presence of a more uniform and homogeneous morphology in the compatibilized polymer blends due to the presence of a compatibilizer.[39,40]

2.6. Crystallization and Melting Behavior by DSC. Differential scanning calorimetry (DSC) measurements have been performed to analyze the melting and crystallization

https://dx.doi.org/10.1021/acsomega.0c00423
ACS Omega 2020, 5, 12789−12808

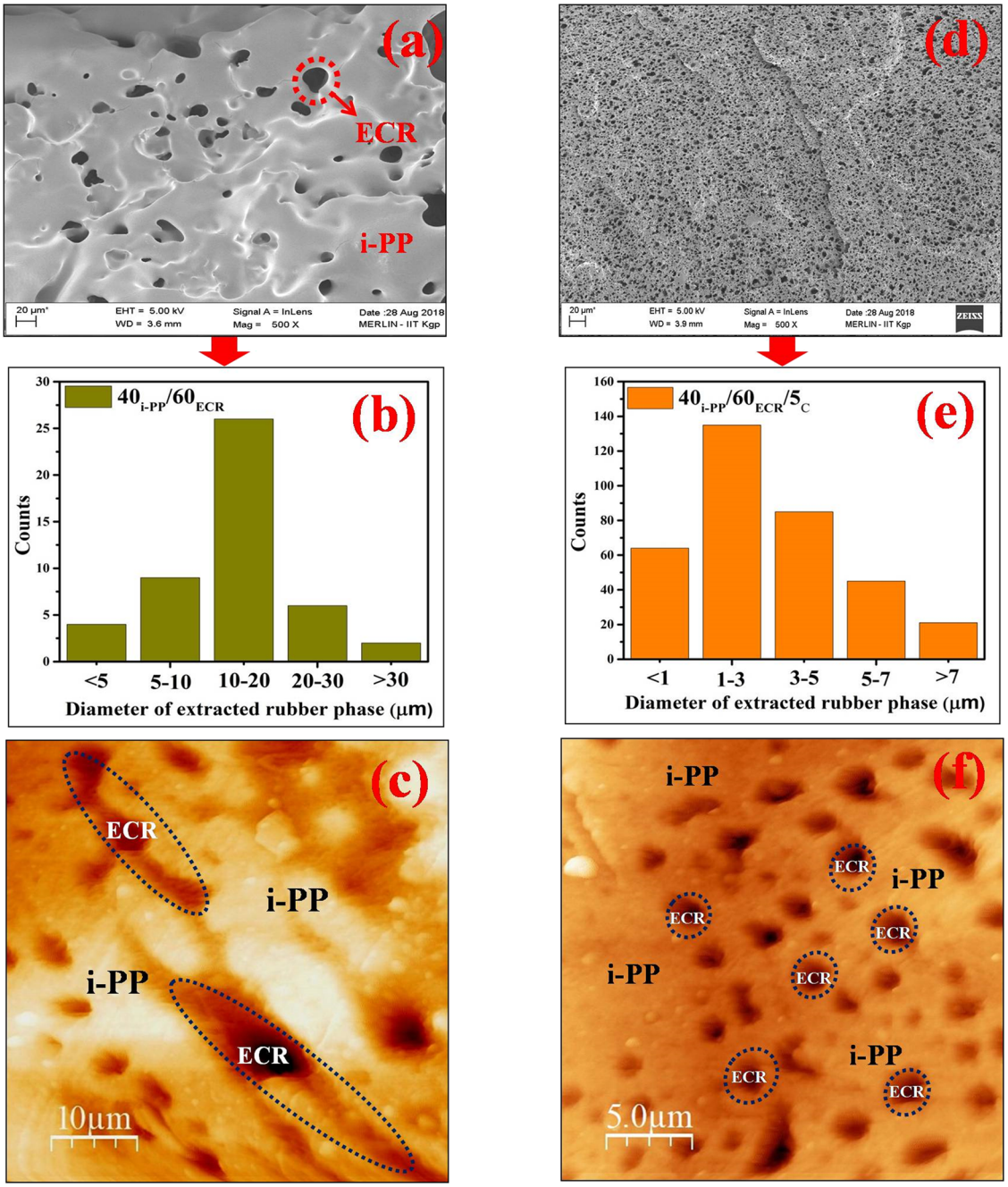

Figure 9. (a) FESEM micrograph of the $40_{i\text{-}PP}/60_{ECR}$ blend, (b) histogram of ECR particle sizes in the $40_{i\text{-}PP}/60_{ECR}$ blend, (c) AFM image of the $40_{i\text{-}PP}/60_{ECR}$ blend, (d) FESEM micrograph of the $40_{i\text{-}PP}/60_{ECR}/5_C$ blend, (e) histogram of ECR particle sizes in the $40_{i\text{-}PP}/60_{ECR}/5_C$ blend, and (f) AFM image of the $40_{i\text{-}PP}/60_{ECR}/5_C$ blend.

behavior of $100_{i\text{-}PP}$ and i-PP/ECR blends ($40_{i\text{-}PP}/60_{ECR}$ and $40_{i\text{-}PP}/60_{ECR}/5_C$). The DSC cooling curves of $100_{i\text{-}PP}$ and i-PP/ECR blends ($40_{i\text{-}PP}/60_{ECR}$ and $40_{i\text{-}PP}/60_{ECR}/5_C$) are shown in Figure 8a. Crystallization parameters such as crystallization onset temperature (T_{OC}), crystallization peak temperature (T_{PC}), and heat of crystallization (ΔH_C) values are reported in Table 5.

The T_{OC}, T_{PC}, and ΔH_C values of the $40_{i\text{-}PP}/60_{ECR}$ blend are lower than those of $100_{i\text{-}PP}$ (Table 5). This indicates that the presence of ECR (rubber/amorphous) in the $40_{i\text{-}PP}/60_{ECR}$ blend hinders the formation of crystals by disrupting the rearrangement of i-PP chains during crystallization, which results in a delayed onset of crystallization (i.e., shifting the crystallization peak to a lower side) in comparison to $100_{i\text{-}PP}$. In the literature, it has been shown that the presence of EPDM rubber (amorphous part) in PP/EPDM blends[41] and the presence of ethylene octene copolymer (EOC) rubber (amorphous part) in PP/EOC blends[42] disrupt the rearrangement of PP chains (hinders the formation of crystals) during crystallization, resulting in a delayed onset of crystallization. The T_{OC}, T_{PC}, and ΔH_C values of the $40_{i\text{-}PP}/60_{ECR}/5_C$ blend are relatively higher than those of the $40_{i\text{-}PP}/60_{ECR}$ blend (Table 5). This shows the enhanced tendency of i-PP to undergo chain folding and recrystallization in the $40_{i\text{-}PP}/60_{ECR}/5_C$ blend due to the presence of the E-AE-MA-TP compatibilizer, which possibly acts as an efficient nucleating

https://dx.doi.org/10.1021/acsomega.0c00423
ACS Omega 2020, 5, 12789−12808

agent. Generally, polyolefin-based compatibilizers (semicrystalline polymers like PP and PE) are added at a very low dosage in polymer blends, which helps in developing crystal growth by behaving like nucleating agents.[17,43,44] There are reports in the literature that examine the nucleating effect of polyolefin-based compatibilizers like MA-PP[17,43] and MA-PE[44] is promoting the crystal growth in PP/ACM blends,[17] PP/NBR blends,[43] and HDPE/NBR blends.[44] Accordingly, here, it is very clear that the ethylene-based E-AE-MA-TP compatibilizer can act as an effective nucleating agent for promoting the crystallization of i-PP chains in the $40_{i\text{-}PP}/60_{ECR}/5_C$ blend, which results in an early onset of crystallization (i.e., shifting the crystallization peak to a higher side) in comparison to the $40_{i\text{-}PP}/60_{ECR}$ blend (Table 5).

The DSC melting curves of $100_{i\text{-}PP}$ and i-PP/ECR blends ($40_{i\text{-}PP}/60_{ECR}$ and $40_{i\text{-}PP}/60_{ECR}/5_C$) show two melting peaks (Figure 8b). The higher melting temperature (T_{HM}) peaks and the lower melting temperature (T_{LM}) peaks seen in all the samples are ascertained to the melting of perfect and disordered crystals of i-PP, respectively.[21,45] The T_{HM} and T_{LM} values of the $40_{i\text{-}PP}/60_{ECR}$ blend and $40_{i\text{-}PP}/60_{ECR}/5_C$ blend are similar to those of $100_{i\text{-}PP}$ (Table 5). In the case of the $40_{i\text{-}PP}/60_{ECR}$ blend, the melting temperatures (T_{HM} and T_{LM}) can come only from the i-PP part and ECR being amorphous will not show any melting behavior. Therefore, the melting temperatures (T_{HM} and T_{LM}) of the $40_{i\text{-}PP}/60_{ECR}$ blend are similar to $100_{i\text{-}PP}$. On the other hand, the melting temperatures (T_{HM} and T_{LM}) of the $40_{i\text{-}PP}/60_{ECR}/5_C$ blend are also similar to those of $100_{i\text{-}PP}$. The melting temperatures (T_{HM} and T_{LM}) of the $40_{i\text{-}PP}/60_{ECR}/5_C$ blend will also come from the i-PP part, and there will not be any influence from the amorphous ECR part. Surprisingly, the presence of the E-AE-MA-TP compatibilizer in the $40_{i\text{-}PP}/60_{ECR}/5_C$ blend also does not show any influence on the melting temperatures (T_{HM} and T_{LM}), which may be due to the presence of a very low dosage of E-AE-MA-TP compatibilizers in the $40_{i\text{-}PP}/60_{ECR}/5_C$ blend.

The degree of crystallinity (X_C (%)) values of $100_{i\text{-}PP}$ and i-PP/ECR blends ($40_{i\text{-}PP}/60_{ECR}$ and $40_{i\text{-}PP}/60_{ECR}/5_C$) are calculated using eq 7, and the calculated X_C (%) values are shown in Table 5. The X_C (%) and ΔH_M values of the $40_{i\text{-}PP}/60_{ECR}$ blend are lower than those of $100_{i\text{-}PP}$, which is due to the presence of ECR (amorphous phase) in the i-PP matrix (Table 5). ECR being amorphous in nature suppresses the ΔH_M of i-PP, which results in the reduction of X_C (%). In the literature, it has been shown that the presence of NR (amorphous part) in PP/NR blends[1] and the presence of EPDM rubber (amorphous part) in PP/EPDM blends[41] result in a concomitant decrease in the enthalpy and degree of crystallinity due to the diluent effect of the amorphous part in the respective blend systems. The X_C (%) and ΔH_M values of the $40_{i\text{-}PP}/60_{ECR}/5_C$ blend are relatively higher than those of the $40_{i\text{-}PP}/60_{ECR}$ blend (Table 5). This is attributed to the nucleating effect of the E-AE-MA-TP compatibilizer in the $40_{i\text{-}PP}/60_{ECR}/5_C$ blend, which increases the ΔH_M of i-PP and leads to enhanced crystal growth and higher X_C (%). In the literature, Soares et al. have shown that the incorporation of MA-PP/TETA as compatibilizers in PP/ACM blends results in a concomitant increase in the ΔH_M and X_C (%) values due to the nucleating effect of the compatibilizers.[17]

2.7. Morphological Studies. Figure 9a shows the FESEM micrograph taken from the etched fractured surface of the $40_{i\text{-}PP}/60_{ECR}$ blend. The black holes in the FESEM micrograph correspond to the etched out ECR phase from the i-PP matrix. It can be seen that the wide and irregularly sized ECR domains are dispersed in the continuous i-PP matrix and the size of the dispersed ECR domains are in between 10 and 20 μm (Figure 9a). The average domain size of the dispersed ECR in the i-PP matrix of the $40_{i\text{-}PP}/60_{ECR}$ blend is 15.8 μm (Figure 9a). The histogram of the distribution of the ECR domain diameter in the i-PP matrix of the $40_{i\text{-}PP}/60_{ECR}$ blend is shown in Figure 9b. The AFM topographic image of the $40_{i\text{-}PP}/60_{ECR}$ blend also shows the dispersion of wide and irregular ECR domains in the i-PP matrix, and the size of the ECR domains (dispersed phase) is between 10 and 20 μm (Figure 9c). The above findings clearly confirm the poor compatibility/interaction between i-PP and ECR in the $40_{i\text{-}PP}/60_{ECR}$ blend. The contact angle studies (discussed earlier) show that the interfacial tension value between i-PP and ECR is 22.15 mN m^{-1}, which is very high and confirms the poor compatibility between i-PP and ECR (Table 1). The FTIR studies (discussed earlier) also confirm the lack of any type of interaction between i-PP and ECR in the $40_{i\text{-}PP}/60_{ECR}$ blend. The poor interfacial adhesion/interaction between i-PP and ECR in the $40_{i\text{-}PP}/60_{ECR}$ blend generates a weaker interface that results in low mechanical properties (as discussed earlier) due to poor stress transfer between the phases while stretching. In the literature, there are many reports that discuss the effect of poor interfacial interaction/adhesion between the incompatible blend components on the mechanical properties of polymer blends.[22,46−48] These include studies on various noncompatibilized polymer blends such as PP/NBR blends,[22] poly(trimethylene terephthalate) (PTT)/EPDM blends,[46] PP/nylon 6 blends,[47] and poly(methyl methacylate) (PMMA)/NR blends.[48] All these noncompatibilized polymer blends have been found to show poor mechanical properties due to weak interfacial interaction/adhesion between the blend components (owing to the wider difference in polarity between the blend components).[22,46−48]

Figure 9d shows the FESEM micrograph taken from the etched fractured surface of the $40_{i\text{-}PP}/60_{ECR}/5_C$ blend. It can be seen that the $40_{i\text{-}PP}/60_{ECR}/5_C$ blend exhibits a more homogeneous morphology and the size of the ECR domains (dispersed phase) is between 1 and 3 μm (Figure 9d). The average domain size of the dispersed ECR in the i-PP matrix of the $40_{i\text{-}PP}/60_{ECR}/5_C$ blend is 1.58 μm (Figure 9d). The histogram of the distribution of the ECR particle diameter in the i-PP matrix of the $40_{i\text{-}PP}/60_{ECR}/5_C$ blend is shown in Figure 9e. The AFM topographic image of the $40_{i\text{-}PP}/60_{ECR}/5_C$ blend also shows the dispersion of more homogeneous ECR domains in the i-PP matrix and the size of the ECR domains (dispersed phase) is between 1 and 3 μm (Figure 9f). It should be pointed out here that the particle size of the ECR domains in the i-PP matrix of the $40_{i\text{-}PP}/60_{ECR}/5_C$ blend is around 90% lower in comparison to the particle size of the ECR domains in the i-PP matrix of the $40_{i\text{-}PP}/60_{ECR}$ blend. The above findings clearly suggest the enhanced compatibility between i-PP and ECR in the $40_{i\text{-}PP}/60_{ECR}/5_C$ blend due to the presence of the E-AE-MA-TP compatibilizer. The contact angle studies (discussed earlier) show that the interfacial tension values between i-PP/E-AE-MA-TP (4.29 mN m^{-1}) and ECR/E-AE-MA-TP (6.96 mN m^{-1}) are relatively very low when compared to the interfacial tension value between i-PP and ECR (22.15 mN m^{-1}) (Table 1). Also, the interfacial tension values between i-PP/E-AE-MA-TP and ECR/E-AE-MA-TP are very close to each other. Accordingly, it is clear that the E-AE-MA-TP compatibilizer can act as an efficient compatibilizer for improving the interfacial interaction between i-PP and ECR.

https://dx.doi.org/10.1021/acsomega.0c00423
ACS Omega 2020, 5, 12789−12808

The FTIR studies (discussed earlier) also confirm the existence of multifaceted interactions between the E-AE-MA-TP compatibilizer with i-PP and ECR in the $40_{i\text{-}PP}/60_{ECR}/5_C$ blend. The enhanced interfacial adhesion/interaction between i-PP and ECR in the $40_{i\text{-}PP}/60_{ECR}/5_C$ blend in the presence of the E-AE-MA-TP compatibilizer facilitates the stress transfer across the interface and leads to a significant improvement in the overall properties (as discussed earlier). In the literature, there are several studies that report the effect of various compatibilizers in improving the interfacial adhesion/interaction between different incompatible polymer blend partners, which eventually leads to enhanced properties.[22,46−48] These include the studies of George et al.,[22] Aravind et al.,[46] Chow et al.,[47] and Oommen et al.,[48] who examined the role of compatibilizers like MA-PP,[22] Ph-PP,[22] m-EPR,[46,47] and NR-g-PMMA[48] in improving the compatibility between various incompatible blend components such as PP/NBR,[22] PTT/EPDM,[46] PP/nylon 6,[47] and PMMA/NR.[48] In all the reported studies, the addition of a compatibilizer significantly reduces the particle size of the dispersed phase.[22,46−48] This has been ascribed to the enhanced interaction between the incompatible blend components due to the presence of a compatibilizer, which in turn leads to a significant improvement in the overall properties.[22,46−48]

The rheological studies (discussed earlier) show that the complex viscosity of the $40_{i\text{-}PP}/60_{ECR}/5_C$ blend is higher than that of the $40_{i\text{-}PP}/60_{ECR}$ blend due to the enhanced interactions between i-PP and ECR in the presence of the E-AE-MA-TP compatibilizer. This correlates well with the remarkably smaller particle size of ECR domains in the i-PP matrix of the $40_{i\text{-}PP}/60_{ECR}/5_C$ blend in comparison to the very larger particle size of ECR domains in the i-PP matrix of the $40_{i\text{-}PP}/60_{ECR}$ blend. Similar to the above observations, there are reports in the literature that discuss the correlation between the rheological behavior (change in viscosity) and morphological properties (change in particle size of the dispersed phase) for PP/NBR blends compatibilized with Ph-PP,[49] nylon 6/acrylonitrile butadiene styrene blends compatibilized with ethylene *n*-butyl acrylate carbon monoxide maleic anhydride,[50] linear low-density polyethylene (LLDPE)/EVA blends compatibilized with phenolic-modified LLDPE or maleic-modified LLDPE,[51] and PTT/EPDM blends compatibilized with EPM-*g*-MA.[52]

3. CONCLUSIONS

This work attempts to understand the effect of a compatibilizer that can have multiple interaction points with incompatible polymer blend components for developing TPEs with significantly improved properties. Accordingly, an E-AE-MA-TP compatibilizer having ethylene groups, acrylic groups, and anhydride/acid groups along its main chain has been successfully used as a compatibilizer for developing TPEs based on nonpolar i-PP and polar ECR. Contact angle studies and FTIR spectroscopy studies confirm that there exists a wide difference in polarity between i-PP and ECR, which suggests the poor compatibility/interaction between i-PP and ECR. The interfacial tension values among i-PP/ECR (22.15 mN m^{-1}), i-PP/E-AE-MA-TP (4.29 mN m^{-1}), and ECR/E-AE-MA-TP (6.96 mN m^{-1}) derived from contact angle studies elucidate that E-AE-MA-TP can act as an efficient compatibilizer for improving the compatibility between i-PP and ECR. FTIR spectroscopy studies confirm the efficacy of the E-AE-MA-TP compatibilizer to establish multifaceted chemical interactions with both i-PP and ECR. The multifaceted interactions of the E-AE-MA-TP compatibilizer with i-PP and ECR have led to enhanced interfacial adhesion between i-PP and ECR, which facilitates stress transfer between the phases and provides remarkable improvement in the mechanical properties. The $40_{i\text{-}PP}/60_{ECR}/5_C$ blend shows a very good tensile strength value (17.2 MPa) and remarkably higher strain at break value (370%) in comparison to the tensile strength value (13.8 MPa) and strain at break value (46%) of the $40_{i\text{-}PP}/60_{ECR}$ blend. In addition, the tension value of the $40_{i\text{-}PP}/60_{ECR}/5_C$ blend is very low in comparison to the tension set value of $40_{i\text{-}PP}/60_{ECR}$ blend because of the better interaction between i-PP and ECR in the presence of the E-AE-MA-TP compatibilizer. This shows the improved elastic recovery behavior of the $40_{i\text{-}PP}/60_{ECR}/5_C$ blend in comparison to that of the $40_{i\text{-}PP}/60_{ECR}$ blend. The $40_{i\text{-}PP}/60_{ECR}/5_C$ blend exhibits a higher mixing torque when compared to the mixing torque of the $40_{i\text{-}PP}/60_{ECR}$ blend due to the occurrence of interactions between i-PP and ECR through the E-AE-MA-TP compatibilizer. The rheological studies (temperature sweep studies) show that the T_g value corresponding to i-PP in the $40_{i\text{-}PP}/60_{ECR}/5_C$ blend occurs at a lower temperature (toward the T_g of ECR) when compared to the T_g value corresponding to i-PP in the $40_{i\text{-}PP}/60_{ECR}$ blend, which is due to the homogeneous mixing between i-PP and ECR in the presence of the E-AE-MA-TP compatibilizer. Also, the tan δ peak height values corresponding to i-PP and ECR in the $40_{i\text{-}PP}/60_{ECR}/5_C$ blend are lower when compared to the tan δ peak height values corresponding to i-PP and ECR in the $40_{i\text{-}PP}/60_{ECR}$ blend, which is due to the enhanced restriction in the mobility of i-PP and ECR chains in the presence of the E-AE-MA-TP compatibilizer. On the other hand, the storage modulus (at 25 °C) value (247 MPa) of the $40_{i\text{-}PP}/60_{ECR}/5_C$ blend is higher in comparison to the storage modulus (at 25 °C) value (214 MPa) of the $40_{i\text{-}PP}/60_{ECR}$ blend, which agrees well with the results obtained from tensile stress−strain studies. The rheological studies (frequency sweep studies) across the entire range of frequencies show that the complex viscosity of the $40_{i\text{-}PP}/60_{ECR}/5_C$ blend is higher than the complex viscosity of the $40_{i\text{-}PP}/60_{ECR}$ blend, which verifies the better interaction between i-PP and ECR in the presence of the E-AE-MA-TP compatibilizer. In addition, the Cole−Cole plot (plot of η'' vs η') of the $40_{i\text{-}PP}/60_{ECR}/5_C$ blend shows a perfect semicircular curve in comparison to that of the $40_{i\text{-}PP}/60_{ECR}$ blend. This is attributed to the presence of a more uniform and homogeneous morphology in the $40_{i\text{-}PP}/60_{ECR}/5_C$ blend in comparison to that of the $40_{i\text{-}PP}/60_{ECR}$ blend. This is because of the enhanced interaction between i-PP and ECR in the $40_{i\text{-}PP}/60_{ECR}/5_C$ blend due to the presence of the E-AE-MA-TP compatibilizer. From DSC studies, it is seen that the $40_{i\text{-}PP}/60_{ECR}/5_C$ blend shows a higher degree of crystallinity and greater tendency to crystallize (early onset of crystallization) in comparison to the $40_{i\text{-}PP}/60_{ECR}$ blend. This is due to the nucleating effect of the E-AE-MA-TP compatibilizer helping in improving the melting and crystallization behavior of the $40_{i\text{-}PP}/60_{ECR}/5_C$ blend. Morphological studies by FESEM and AFM show that the particle size of the ECR domains (dispersed phase) in the i-PP matrix of the $40_{i\text{-}PP}/60_{ECR}/5_C$ blend is remarkably smaller (∼90% smaller) when compared to the particle size of the ECR domains (dispersed phase) in the i-PP matrix of the $40_{i\text{-}PP}/60_{ECR}$ blend. This is because of the enhanced interfacial adhesion between i-PP and ECR in the $40_{i\text{-}PP}/60_{ECR}/5_C$ blend due to the presence of the E-AE-MA-TP compatibilizer. Finally, it is concluded that the E-AE-

https://dx.doi.org/10.1021/acsomega.0c00423
ACS Omega 2020, 5, 12789−12808

Table 6. Comparison of Ultimate Tensile Strength, Strain at Break, and Degree of Crystallinity Values of Compatibilized $40_{i\text{-}PP}/60_{ECR}/5_C$ Blend (Documented in This Article) with Some of the PP- and Polar Elastomer-Based TPEs (with Different Compatibilizers) Reported in the Literature[a]

sl. no.	TPEs	compatibilizing agent	ultimate tensile strength (MPa)	strain at break (%)	degree of crystallinity (X_C (%)) by DSC	ref
1	50PP/50ACM/5MA-PP/0.5TETA	MA-PP (5 wt %) and TETA (0.5 wt %)	15.9	340	38.6	17
2	60PP/100m-EPM/10MA-PP	MA-PP (10 wt %)	3.5	120		20
3	50DPM-PP/50NBR	technological compatibilization	10.1	66		23
4	40PP/60NBRr/1ER	ER (1 phr)	5	6.5		19
5	$40_{i\text{-}PP}$/60ECR/5MA-PP	MA-PP (5 wt %)	15.5	138	39.8	21
6	$40_{i\text{-}PP}/60_{ECR}/5_C$	E-AE-MA-TP (5 wt %)	17.2	370	42.1	this paper

[a]PP represents polypropylene, ACM represents acrylic rubber, MA-PP represents maleic anhydride-grafted polypropylene, TETA represents triethylene tetramine, m-EPM represents maleated ethylene propylene rubber, DPM-PP represents dimethylol phenolic-modified polypropylene, NBRr represents recycled acrylonitrile butadiene rubber, ER represents epoxy resin, ECR represents epichlorohydrin rubber, and E-AE-MA-TP represents the ethylene-acrylic ester-maleic anhydride terpolymer.

MA-TP compatibilizer is capable of generating multiple point interactions within the i-PP/ECR blend, which leads to the development of TPEs having properties that are much more outstanding than several compatibilized TPEs (based on PP and polar elastomers) reported in the literature. A summary of some important properties of the i-PP/ECR blend compatibilized with the E-AE-MA-TP compatibilizer reported in this paper along with the properties of other compatibilized TPEs (based on PP and polar elastomers) reported in the literature is shown in Table 6 and Figure 10a,b, which clearly validates our argument.

4. EXPERIMENTAL SECTION

4.1. Materials. Epichlorohydrin homopolymers (grade name Hydrin H55, CAS number:24969-06-0) having a density of 1.37 g/cm^3 at 25 °C and Mooney viscosity of 54 (ML_{1+4} at 100 °C) were provided by Zeon Chemicals, USA. Isotactic polypropylene homopolymers (grade name AM120N, CAS number:9003-07-0) having a melt flow rate of 12 g/10 min (2.16 kg at 230 °C), density of 0.91 g/cm^3, and melting point of 165 °C were provided by Reliance Industries Ltd., India. Ethylene-acrylic ester-maleic anhydride terpolymers (grade name LOTADER 4700, CAS number:41171-14-6) having an ethyl acrylate content of 29 wt %, maleic anhydride content of 1.3 wt %, density of 0.94 g/cm^3, melting point of 65 °C, and melt flow rate of 7 g/10 min (2.16 kg at 190 °C) were purchased from Arkema Chemicals, France. The chemical structures of the blend components (i-PP and ECR) and compatibilizer (E-AE-MA-TP) are given in Figure 11.

4.2. Blend Preparation. The materials were dried in a vacuum oven (i-PP was dried for 3 h at 80 °C and E-AE-MA-TP compatibilizer was dried for 3 h at 40 °C) before melt mixing. Melt mixing of the neat samples (i-PP and ECR) and blends were carried out on a counter-rotating Haake Rheocord internal mixer (Thermo Fisher Scientific, Germany) having two roller-type rotors. The internal mixer temperature was kept at 190 °C. A constant rotor speed of 100 rpm was used during mixing. Neat i-PP and neat ECR samples were prepared by mixing i-PP or ECR for 7 min in the internal mixer. Then, i-PP or ECR was taken out in the molten state from the internal mixer and sheeted out at room temperature using a two roll mixing mill (Santec mixing mill, 6X13, India) having a 2 mm nip gap to form a uniform sheet having a 2 mm thickness. The various pristine samples prepared are depicted in Table 7. In the case of noncompatibilized blend samples, first, i-PP was mixed for 2 min in the internal mixer followed by the addition of ECR. Then, i-PP and ECR was allowed to blend for 5 min. The i-PP/ECR blend was taken out in the molten state from the internal mixer and sheeted out at room temperature using a two roll mixing mill having a 2 mm nip gap to form a uniform sheet having a 2 mm thickness. The detailed steps involved in the preparation of the noncompatibilized i-PP/ECR blend are shown in Figure 12a. The various noncompatibilized blends prepared are depicted in Table 7. In the case of blends having a compatibilizer, first, i-PP was mixed for 1 min in the internal mixer followed by the addition of the E-AE-MA-TP compatibilizer. Then, the blending of i-PP and the E-AE-MA-TP compatibilizer was continued for another 2 min. Finally, ECR was added and allowed to blend for 5 min. The i-PP/ECR/E-AE-MA-TP blend was taken out in the molten state from the internal mixer and sheeted out at room temperature using a two roll mixing mill having a 2 mm nip gap to form a uniform sheet having a 2 mm thickness. The detailed steps involved in the preparation of the i-PP/ECR blend in the presence of the E-AE-MA-TP compatibilizer are shown in Figure 12b. The various compatibilized blends prepared are depicted in Table 7. Neat i-PP, noncompatibilized blends, and compatibilized blends were molded in a Haake MiniJet-II microinjection molding machine (Thermo Scientific, Germany). The mold and cylinder temperatures were 50 and 220 °C, respectively, the injection pressure and injection time were 450 bar and 5 s, respectively, and the holding pressure and holding time were 200 bar and 7 s, respectively.

4.3. Characterization Techniques. *4.3.1. Surface and Interface Property Analyses by Contact Angle Measurements.* The values of the polar (γ_S^P) and dispersion (γ_S^D) components of surface energy for the samples were obtained using a Rame-Hart goniometer (model no. 250-F1, USA). A sessile drop method employing 20 μL drops of different probe liquids was used for the contact angle measurements. All the contact angle measurements were performed in a vapor-saturated atmosphere (air) at room temperature. Distilled water, formamide (FM), dimethylsulfoxide (DMSO), and ethylene glycol (EG) were used as the probe liquids for contact angle measurements. FM, DMSO, and EG were procured from Sigma-Aldrich, New Delhi, India. Each contact angle quoted was the average of 10 measurements with a standard deviation in θ of ±1°. The values of the dispersion and polar

https://dx.doi.org/10.1021/acsomega.0c00423
ACS Omega 2020, 5, 12789−12808

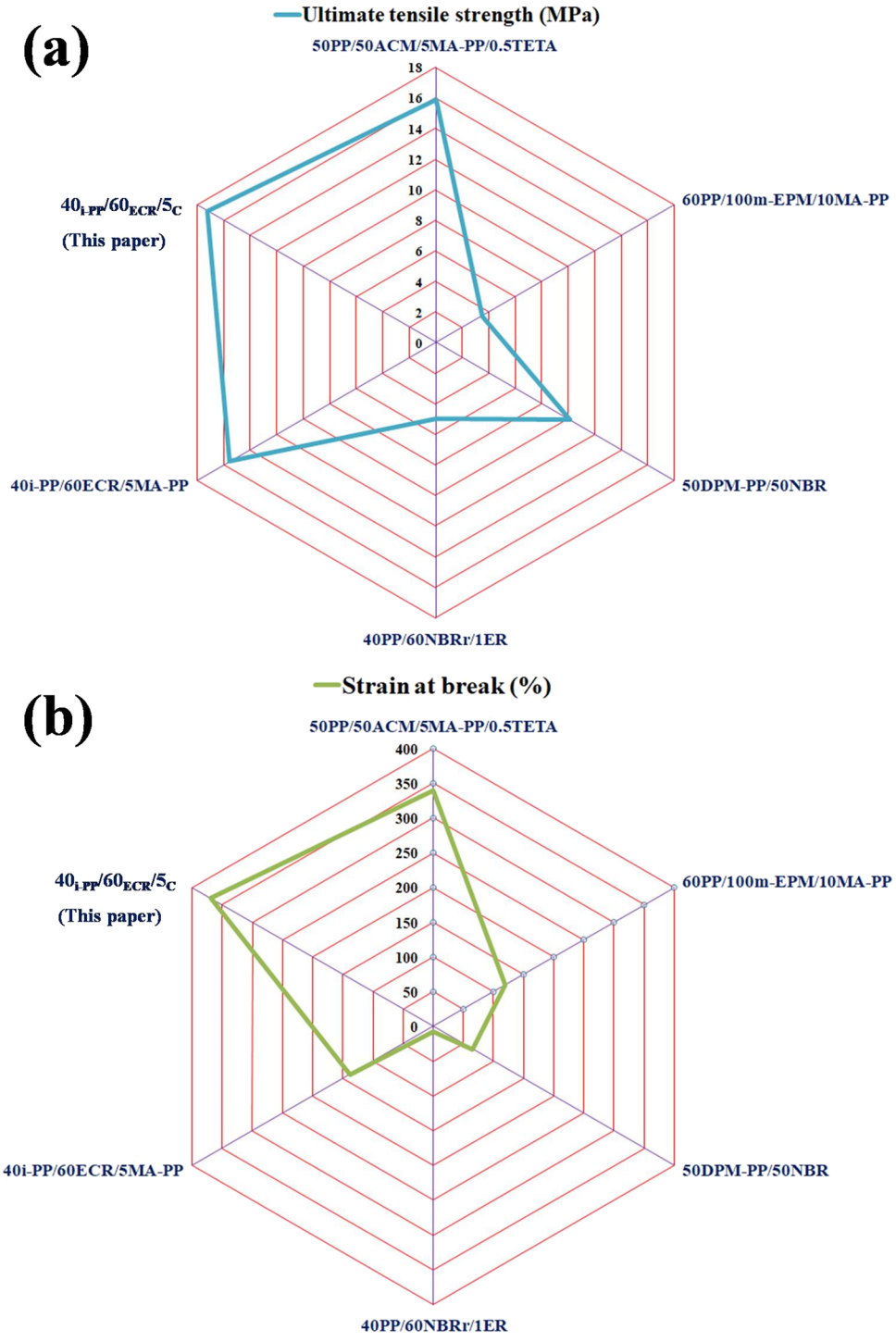

Figure 10. (a) Evaluation of ultimate tensile strength of the compatibilized $40_{i\text{-}PP}/60_{ECR}/5_C$ blend (documented in this article) with some of the PP- and polar elastomer-based TPEs (with different compatibilizers) reported in the literature and (b) evaluation of strain at break of the compatibilized $40_{i\text{-}PP}/60_{ECR}/5_C$ blend (documented in this article) with some of the PP- and polar elastomer-based TPEs (with different compatibilizers) reported in the literature.

components of the various probe liquids used in this study are listed in Table 8.

The dispersion (γ_S^D) and polar (γ_S^P) components of $100_{i\text{-}PP}$, 100_{ECR}, and the E-AE-MA-TP compatibilizer have been calculated using the contact angles of different probe liquids on the sample surfaces in accordance with the following theory. The Young equation for the contact angle θ can be written as[53,55]

$$\gamma_S = \gamma_{SL} + \gamma_L \cos\theta \quad (1)$$

where γ_S represents the surface free energy of the solid, γ_L represents the surface free energy of the liquid, and γ_{SL} represents the surface free energy of the solid−liquid interface.

The surface energies of both the solid and liquid can be given as the sum of polar components (denoted by superscript P) and dispersive components (denoted by superscript D) as shown below

https://dx.doi.org/10.1021/acsomega.0c00423
ACS Omega 2020, 5, 12789−12808

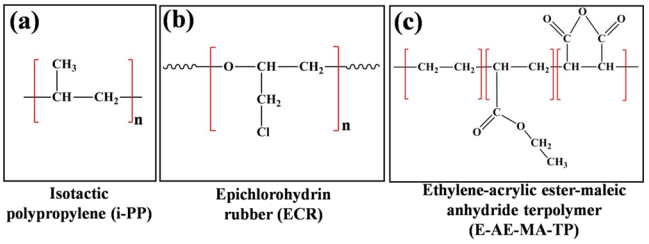

Figure 11. Chemical structure of (a) i-PP, (b) ECR, and (c) the E-AE-MA-TP compatibilizer.

Table 7. Sample Compositions and Notations

sl. no.	samples	i-PP (wt %)	ECR (wt %)	compatibilizer (E-AE-MA-TP) (wt %)
1	$100_{i\text{-}PP}$	100	0	0
2	100_{ECR}	0	100	0
3	$50_{i\text{-}PP}/50_{ECR}$	50	50	0
4	$40_{i\text{-}PP}/60_{ECR}$	40	60	0
5	$30_{i\text{-}PP}/70_{ECR}$	30	70	0
6	$20_{i\text{-}PP}/80_{ECR}$	20	80	0
7	$40_{i\text{-}PP}/60_{ECR}/3_C$	40	60	3
8	$40_{i\text{-}PP}/60_{ECR}/5_C$	40	60	5
9	$40_{i\text{-}PP}/60_{ECR}/7_C$	40	60	7
10	$30_{i\text{-}PP}/70_{ECR}/3_C$	30	70	3
11	$30_{i\text{-}PP}/70_{ECR}/5_C$	30	70	5
12	$30_{i\text{-}PP}/70_{ECR}/7_C$	30	70	7

$$\gamma_S = \gamma_S^D + \gamma_S^P \quad (2)$$

Table 8. Literature Data of Probe Liquids Used in Contact Angle Studies

sl. no.	liquids	γ_S^P (mN m^{-1})	γ_S^D (mN m^{-1})	γ_S (mN m^{-1})	ref
1	water	51.0	21.8	72.8	53
2	ethylene glycol	19.0	29.3	48.3	54
3	formamide	18.7	39.5	58.2	54
4	dimethyl sulfoxide	8.68	34.86	43.54	53

$$\gamma_L = \gamma_L^D + \gamma_L^P \quad (3)$$

The Fowkes equation for the surface free energies of the two solid surfaces can be written as[53]

$$\gamma_{SL} = \gamma_S + \gamma_L - 2(\gamma_S^D \gamma_L^D)^{1/2} - 2(\gamma_S^P \gamma_L^P)^{1/2} \quad (4)$$

Combining eq 1 and eq 4 gives

$$\frac{\gamma_L(1+\cos\theta)}{2(\gamma_L^D)^{1/2}} = (\gamma_S^P)^{1/2}\frac{(\gamma_L^P)^{1/2}}{(\gamma_L^D)^{1/2}} + (\gamma_S^D)^{1/2} \quad (5)$$

The graph based on the plot between $\frac{\gamma_L(1+\cos\theta)}{2(\gamma_L^D)^{1/2}}$ and $\frac{(\gamma_L^P)^{1/2}}{(\gamma_L^D)^{1/2}}$ will be linear with $(\gamma_S^D)^{1/2}$ as the intercept and $(\gamma_S^P)^{1/2}$ as the slope.

The interfacial tension values between the blend components have also been calculated using the Owens−Wendt equation as shown below[56,57]

$$\gamma_{12} = \gamma_1 + \gamma_2 - 2[(\gamma_1^D \gamma_2^D)^{1/2} + (\gamma_1^P \gamma_2^P)^{1/2}] \quad (6)$$

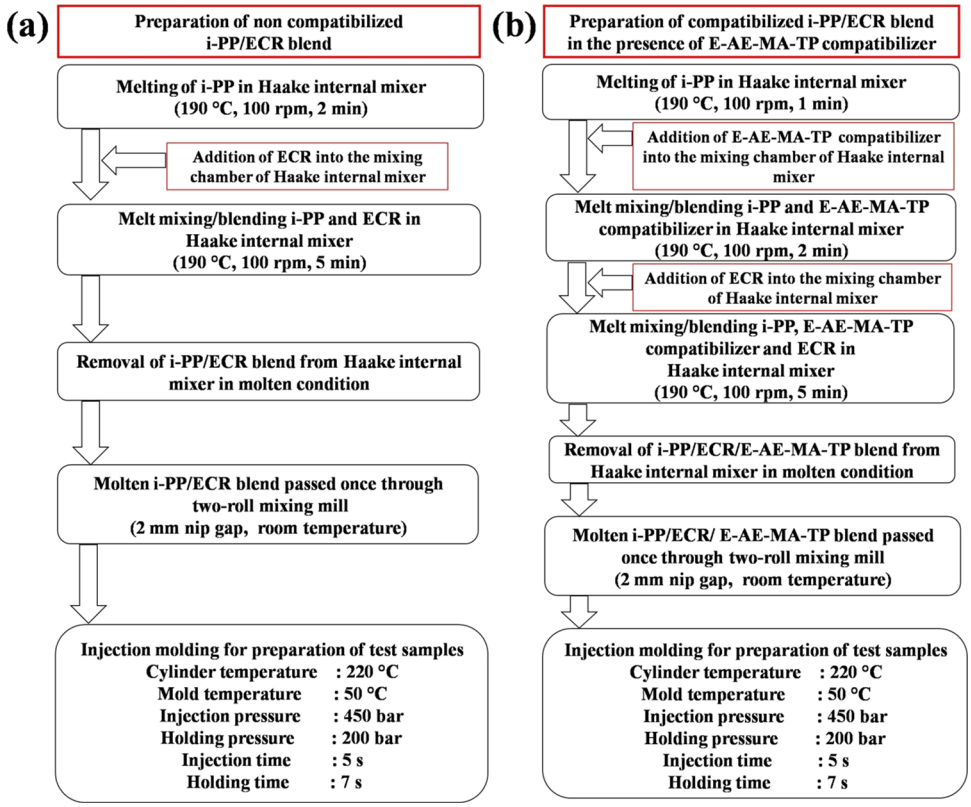

Figure 12. Schematic diagram of the preparation of the (a) noncompatibilized i-PP/ECR blend and (b) compatibilized i-PP/ECR blend (in the presence of E-AE-MA-TP compatibilizer).

https://dx.doi.org/10.1021/acsomega.0c00423
ACS Omega 2020, 5, 12789−12808

where γ_{12} represents the interfacial tension between 1 and 2 (1 and 2 represent interfacial tension between either i-PP/ECR or i-PP/E-AE-MA-TP or ECR/E-AE-MA-TP),

γ_1 represents the surface free energy of 1 (1 represents either i-PP, ECR, or E-AE-MA-TP compatibilizer),

γ_2 represents the surface free energy of 2 (2 represents either i-PP, ECR, or E-AE-MA-TP compatibilizer), γ_1^D and γ_2^D represent dispersive components of the surface free energy for 1 and 2, respectively, and

γ_1^P and γ_2^P represent polar components of the surface free energy for 1 and 2, respectively.

4.3.2. Fourier Transform Infrared (FTIR) Spectroscopy Studies. The infrared spectroscopy of the samples was recorded by Fourier transform infrared spectroscopy (FTIR, IRAffinity-1S, Shimadzu, Japan) in attenuated total reflection (ATR) mode. The samples were scanned from 4000 to 500 cm^{-1} with a resolution of 4 cm^{-1}.

4.3.3. Tensile Stress–Strain Properties. The tensile test of the samples was carried out in a universal testing machine (UTM, Zwick-Roell Z010, Germany) at 25 °C at a test speed of 100 mm/min. The samples were prepared according to ISO 527-2-5A specification. The average values of five samples per batch were reported here. To understand the rubbery nature (recovery nature) of the noncompatibilized blends and compatibilized blends, tension set measurements were performed by stretching the samples to 50% elongation (along tensile direction) at a rate of 100 mm/min and the samples were kept at that position for 10 min. The samples were allowed to relax back to the unstressed condition. The percentage change in the dimensions of the samples in the tensile direction was measured after 24 h and reported as the tension set. The tension set experiments were performed according to ASTM D412-98 specification. The average values of five samples per batch were reported here.

4.3.4. Rheological Studies. 4.3.4.1. Viscoelasticity Studies. Viscoelastic properties were measured using a modular compact rheometer (MCR 302, Anton Paar Austria). The experiments were performed in a torsion-mode geometry at a constant frequency of 1 Hz, constant strain of 0.01%, and temperature ranging from −100 to +100 °C with a heating rate of 2 °C/min.

4.3.4.2. Frequency Sweep Studies. Rheological properties were studied using a modular compact rheometer (MCR 302, Anton Paar Austria). The experiments were performed in a parallel plate geometry with a plate diameter of 25 mm and a gap of 1 mm. Frequency sweep tests were carried out from high to low frequencies (600–0.1 rad s^{-1}). In all the cases, the applied strain was 5% (selected from the linear viscoelastic region of the strain sweep curves) and all the measurements were performed at 190 °C.

4.3.5. Differential Scanning Calorimetry Studies. Melting and crystallization behaviors of the samples were studied using a differential scanning calorimeter (DSC 250, TA Instrument, USA). The samples were first heated at a rate of 10 °C/min from 25 to 200 °C and kept at this temperature (200 °C) for 5 min to eliminate the thermal history. Afterward, the samples were cooled to 25 °C at a rate of 10 °C/min and held at 25 °C for 5 min. Finally, the samples were reheated again to 200 °C at a rate of 2 °C/min. All runs were carried out under a nitrogen (N_2) atmosphere (at a gas flow rate of 50 mL/min) to prevent thermal degradation of samples. The degree of crystallinity (X_C (%)) values of the samples was calculated using the following equation[21,40,58]

$$X_C\ (\%) = \frac{\Delta H_M}{\Delta H_M^{\circ}(1 - \propto)} \times 100 \quad (7)$$

where, ΔH_M is the experimentally obtained second melting enthalpy value of the sample (J g^{-1}), $(1 - \propto)$ is the weight percent of i-PP in the sample, and ΔH_M° is the enthalpy value of melting of a 100% crystalline form of i-PP (209 J g^{-1}).[21,40,58]

4.3.6. Morphological Studies. 4.3.6.1. Field Emission Scanning Electron Microscopy (FESEM). Scanning electron microscopy of the samples was performed using a field emission scanning electron microscope (FESEM, Supra 40 Carl Zeiss, Germany). The samples were cryofractured, and the rubber (ECR) phase was preferentially extracted using chloroform solvent (good solvent for completely dissolving ECR) at room temperature for 5 h following the procedure reported elsewhere.[21,22,29,41,49,50,52] The etched samples were dried in a vacuum oven at 50 °C for 2 h. The dried samples were mounted on metallic studs using double-sided conductive tape and sputter-coated for 60 s with a thin layer of gold in a vacuum at a current intensity of 40 mA using a sputter coating machine (Q150T S sputter coater, Quorum, UK).

4.3.6.2. Atomic Force Microscopy (AFM). Atomic force microscopy (AFM) studies were carried out using an atomic force microscope (Agilent 5500 Scanning Probe Microscope, USA). The AFM imaging was carried out in air at ambient conditions (25 °C) in tapping mode using a long tapping-mode etched silicon probe (LTESP) tip.

AUTHOR INFORMATION

Corresponding Author

Dinesh Kumar Kotnees − *Department of Metallurgical and Materials Engineering, Indian Institute of Technology, Patna 801106, India;* orcid.org/0000-0002-7227-3839; Phone: +916123028185; Email: dineshvnr@gmail.com, dinesh@iitp.ac.in

Authors

Harekrishna Panigrahi − *Department of Metallurgical and Materials Engineering, Indian Institute of Technology, Patna 801106, India*

Paradesiparampil R. Sreenath − *Department of Metallurgical and Materials Engineering, Indian Institute of Technology, Patna 801106, India*

Complete contact information is available at: https://pubs.acs.org/10.1021/acsomega.0c00423

Notes

The authors declare no competing financial interest.

ACKNOWLEDGMENTS

The authors greatly acknowledge Reliance Industries Limited, India for supplying isotactic polypropylene and Zeon Chemicals L.P., USA for supplying the epichlorohydrin homopolymer.

REFERENCES

(1) Choudhury, N. R.; Chaki, T. K.; Bhowmick, A. K. Thermal characterization of thermoplastic elastomeric natural rubber-polypropylene blends. *Thermochim. Acta* **1991**, *176*, 149–161.

(2) Ning, N.; Li, S.; Wu, H.; Tian, H.; Yao, P.; HU, G.-H.; Tian, M.; Zhang, L. Preparation, microstructure, and microstructure-properties relationship of thermoplastic vulcanizates (TPVs): A review. *Prog. Polym. Sci.* **2018**, *79*, 61–97.

(3) Spontak, R. J.; Patel, N. P. Thermoplastic elastomers: Fundamentals and applications. *Curr. Opin. Colloid Interface Sci.* **2000**, *5*, 333−340.
(4) Saleesung, T.; Saeoui, P.; Sirisinha, C. Mechanical and thermal properties of thermoplastic elastomer based on low density polyethylene and ultra-fine fully-vulcanized acrylonitrile butadiene rubber powder (UFNBRP). *Polym. Test.* **2010**, *29*, 977−983.
(5) Ghosh, P.; Chattopadhyay, B.; Sen, A. K. Thermoplastic elastomers from blends of polyethylene and ethylene-propylene-diene rubber: influence of vulcanization technique on phase morphology and vulcanizate properties. *Polymer* **1994**, *35*, 3958−3965.
(6) Banerjee, S. S.; Bhowmick, A. K. Tailored nanostructured thermoplastic elastomers from polypropylene and fluoroelastomer: Morphology and functional properties. *Ind. Eng. Chem. Res.* **2015**, *54*, 8137−8146.
(7) Banerjee, S. S.; Bhowmick, A. K. An effective strategy to develop nanostructured morphology and enhanced physico-mechanical properties of PP/EPDM thermoplastic elastomers. *J. Mater. Sci.* **2016**, *51*, 6722−6734.
(8) Goharpey, F.; Nazockdast, H.; Katbab, A. A. Relationship between the rheology and morphology of dynamically vulcanized thermoplastic elastomers based on EPDM/PP. *Polym. Eng. Sci.* **2005**, *45*, 84−94.
(9) Sengupta, P.; Noordermeer, J. W. M. A comparative study of different techniques for microstructural characterization of oil extended thermoplastic elastomer blends. *Polymer* **2005**, *46*, 12298−12305.
(10) Ismail, H.; Suryadiansyah. Thermoplastic elastomers based on polypropylene/natural rubber and polypropylene/recycle rubber blends. *Polym. Test.* **2002**, *21*, 389−395.
(11) Passador, F. R.; Rojas, G. J. A.; Pessan, L. A. Thermoplastic elastomers based on natural rubber/polypropylene blends: Effect of blend ratios and dynamic vulcanization on rheological, thermal, mechanical, and morphological properties. *J. Macromol. Sci., Part B: Phys.* **2013**, *52*, 1142−1157.
(12) Kuriakose, B.; De, S. K. Studies on the melt flow behavior of thermoplastic elastomers from polypropylene—natural rubber blends. *Polym. Eng. Sci.* **1985**, *25*, 630−634.
(13) Ahmad, Z.; Kumar, K. D.; Saroop, M.; Preschilla, N.; Biswas, A.; Bellare, J. R.; Bhowmick, A. K. Highly transparent thermoplastic elastomer from isotactic polypropylene and styrene/ethylene-butylene/styrene triblock copolymer: structure-property correlations. *Polym. Eng. Sci.* **2010**, *50*, 331−341.
(14) Heidari, A.; Fasihi, M. Cell structure-impact property relationship of polypropylene/thermoplastic elastomer blend foams. *eXPRESS Polym. Lett.* **2019**, *13*, 429−442.
(15) Svoboda, P.; Theravalappil, R.; Svobodova, D.; Mokrejs, P.; Kolomaznik, K.; Mori, K.; Ougizawa, T.; Inoue, T. Elastic properties of polypropylene/ethylene-octene copolymer blends. *Polym. Test.* **2010**, *29*, 742−748.
(16) Cook, R. F.; Koester, K. J.; Macosko, C. W.; Ajbani, M. Rheological and mechanical behavior of blends of styrene-butadiene rubber with polypropylene. *Polym. Eng. Sci.* **2005**, *45*, 1487−1497.
(17) Soares, B. G.; Santos, D. M.; Sirqueira, A. S. A novel thermoplastic elastomer based on dynamically vulcanized polypropylene/acrylic rubber blends. *eXPRESS Polym. Lett.* **2008**, *2*, 602−613.
(18) Pan, J.; Hu, H.; Huang, Z.; Duan, Y. The influence of compatibilizers on nitrile-butadiene rubber and polypropylene (NBR/PP) blends. *Polym.-Plast. Technol. Eng.* **2001**, *40*, 593−604.
(19) Ismail, H.; Galpaya, D.; Ahmad, Z. The compatibilizing effect of epoxy resin (EP) on polypropylene (PP)/recycled acrylonitrile butadiene rubber (NBRr) blends. *Polym. Test.* **2009**, *28*, 363−370.
(20) Chatterjee, K.; Naskar, K. Development of thermoplastic elastomers based on maleated ethylene propylene rubber (m-EPM) and polypropylene (PP) by dynamic vulcanization. *eXPRESS Polym. Lett.* **2007**, *1*, 527−534.
(21) Panigrahi, H.; Sreenath, P. R.; Bhowmick, A. K.; Dinesh Kumar, K. Unique compatibilized thermoplastic elastomer from polypropylene and epichlorohydrin rubber. *Polymer* **2019**, *183*, 121866.
(22) George, S.; Neelakantan, N. R.; Varughese, K. T.; Thomas, S. Dynamic mechanical properties of isotactic polypropylene/ nitrile rubber blends: Effects of blend ratio, reactive compatibilization, and dynamic vulcanization. *J. Polym. Sci., Part B: Polym. Phys.* **1997**, *35*, 2309−2327.
(23) Coran, A. Y.; Patel, R. Rubber-thermoplastic compositions. part viii. nitrile rubber polyolefin blends with technological compatibilization. *Rubber Chem. Technol.* **1983**, *56*, 1045−1060.
(24) Chinnadurai, T.; Arungalai Vendan, S.; Rusu, C. C.; Scutelnicu, E. Experimental investigations on the polypropylene behavior during ultrasonic welding. *Mater. Manuf. Processes* **2018**, *33*, 718−726.
(25) Gaylord, N. G. Compatibilizing agents: structure and function in polyblends. *J. Macromol. Sci., Chem.* **2006**, *26*, 1211−1229.
(26) Benedetti, E.; D'Alessio, A.; Aglietto, M.; Ruggeri, G.; Vergamini, P.; Ciardelli, F. Vibrational analysis of functionalized polyolefins/poly(vinylchloride) blends. *Polym. Eng. Sci.* **1986**, *26*, 9−14.
(27) Teh, J. W.; Rudin, A.; Keung, J. C. A review of polyethylene-polypropylene blends and their compatibilization. *Adv. Polym. Technol.* **1994**, *13*, 1−23.
(28) Setua, D. K.; Soman, C.; Bhowmick, A. K.; Mathur, G. N. Oil resistant thermoplastic elastomers of nitrile rubber and high density polyethylene blends. *Polym. Eng. Sci.* **2002**, *42*, 10−18.
(29) George, S.; Joseph, R.; Thomas, S.; Varughese, K. T. Blends of isotactic polypropylene and nitrile rubber: Morphology, mechanical properties and compatibilization. *Polymer* **1995**, *36*, 4405−4416.
(30) Asami, T.; Nitta, K. H. Morphology and mechanical properties of polyolefinic thermoplastic elastomer I. Characterization of deformation process. *Polymer* **2004**, *45*, 5301−5306.
(31) Tanrattanakul, V.; Kosonmetee, K.; Laokijcharoen, P. Polypropylene/natural rubber thermoplastic elastomer: effect of phenolic resin as a vulcanizing agent on mechanical properties and morphology. *J. Appl. Polym. Sci.* **2009**, *112*, 3267−3275.
(32) Thitithammawong, A.; Noordermeer, J. W. M.; Kaesaman, A.; Nakason, C. Influence of compatibilizers on the rheological, mechanical, and morphological properties of epoxidized natural rubber/polypropylene thermoplastic vulcanizates. *J. Appl. Polym. Sci.* **2008**, *107*, 2436−2443.
(33) Pichaiyut, S.; Nakason, C.; Kaesaman, A.; Kiatkamjornwong, S. Influences of blend compatibilizers on dynamic, mechanical, and morphological properties of dynamically cured maleated natural rubber and high-density polyethylene blends. *Polym. Test.* **2008**, *27*, 566−580.
(34) Soares, B. G.; De Oliveira, M.; Meireles, D.; Sirqueira, A. S.; Mauler, R. S. Dynamically vulcanized polypropylene / nitrile rubber blends : The effect of peroxide / bis-maleimide curing system and different compatibilizing systems. *J. Appl. Polym. Sci.* **2008**, *110*, 3566−3573.
(35) Mathew, M.; Thomas, S. Compatibilisation of heterogeneous acrylonitrile-butadiene rubber/polystyrene blends by the addition of styrene-acrylonitrile copolymer: Effect on morphology and mechanical properties. *Polymer* **2003**, *44*, 1295−1307.
(36) Komalan, C.; George, K. E.; Kumar, P. A. S.; Varughese, K. T.; Thomas, S. Dynamic mechanical analysis of binary and ternary polymer blends based on nylon copolymer/EPDM rubber and EPM grafted maleic anhydride compatibilizer. *eXPRESS Polym. Lett.* **2007**, *1*, 641−653.
(37) Paul, S. A.; Sinturel, C.; Joseph, K.; Mathew, G. D. G.; Pothan, L. A.; Thomas, S. Dynamic mechanical analysis of novel composites from commingled polypropylene fiber and banana fiber. *Polym. Eng. Sci.* **2010**, *50*, 384−395.
(38) John, B.; Varughese, K. T.; Oommen, Z.; Pötschke, P.; Thomas, S. Dynamic mechanical behavior of high-density polyethylene/ethylene vinyl acetate copolymer blends: The effects of the blend ratio, reactive compatibilization, and dynamic vulcanization. *J. Appl. Polym. Sci.* **2003**, *87*, 2083−2099.
(39) Codou, A.; Anstey, A.; Misra, M.; Mohanty, A. K. Novel compatibilized nylon-based ternary blends with polypropylene and

https://dx.doi.org/10.1021/acsomega.0c00423
ACS Omega 2020, 5, 12789−12808

poly(lactic acid): Morphology evolution and rheological behaviour. *RSC Adv.* **2018**, *8*, 15709−15724.
(40) Zanjanijam, A. R.; Hakim, S.; Azizi, H. Morphological, dynamic mechanical, rheological and impact strength properties of the PP/PVB blends: The effect of waste PVB as a toughener. *RSC Adv.* **2016**, *6*, 44673−44686.
(41) Chen, Y.; Xu, C.; Cao, L.; Wang, Y.; Cao, X. PP/EPDM-based dynamically vulcanized thermoplastic olefin with zinc dimethacrylate: preparation, rheology, morphology, crystallization and mechanical properties. *Polym. Test.* **2012**, *31*, 728−736.
(42) Babu, R. R.; Singha, N. K.; Naskar, K. Effects of mixing sequence on peroxide cured polypropylene (PP)/ ethylene octene copolymer (EOC) thermoplastic vulcanizates (TPVs). Part . I . morphological, mechanical and thermal properties. *J. Polym. Res.* **2010**, *17*, 657−671.
(43) Xu, C.; Cao, X.; Jiang, X.; Zeng, X.; Chen, Y. Preparation, structure and properties of dynamically vulcanized polypropylene/acrylonitrile butadiene rubber/zinc dimethacrylate ternary blend composites containing maleic anhydride grafted polypropylene. *Polym. Test.* **2013**, *32*, 507−515.
(44) Ponnamma, D.; George, J.; Thomas, M. G.; Chan, C. H.; Valić, S.; Mozetič, M.; Cvelbar, U.; Thomas, S. Investigation on the thermal and crystallization behavior of high density polyethylene/acrylonitrile butadiene rubber blends and their composites. *Polym. Eng. Sci.* **2015**, *55*, 1203−1210.
(45) Song, Y.; Wang, Y.; Li, H.; Zong, Q.; Xu, A. Role of wood fibers in tuning dynamic rheology, non-isothermal crystallization, and microcellular structure of polypropylene foams. *Materials* **2019**, *12*, 106.
(46) Aravind, I.; Albert, P.; Ranganathaiah, C.; Kurian, J. V.; Thomas, S. Compatibilizing effect of EPM-g-MA in EPDM/poly(trimethylene terephthalate) incompatible blends. *Polymer* **2004**, *45*, 4925−4937.
(47) Chow, W. S.; Abu Bakar, A.; Mohd Ishak, Z. A.; Karger-Kocsis, J.; Ishiaku, U. S. Effect of maleic anhydride-grafted ethylene-propylene rubber on the mechanical, rheological and morphological properties of organoclay reinforced polyamide 6/polypropylene nanocomposites. *Eur. Polym. J.* **2005**, *41*, 687−696.
(48) Oommen, Z.; Gopinathan Nair, M. R.; Thomas, S. Compatibilizing effect of natural rubber-g-poly(methyl methacrylate) in heterogeneous natural rubber/poly(methyl methacrylate) blends. *Polym. Eng. Sci.* **1996**, *36*, 151−160.
(49) George, S.; Ramamurthy, K.; Anand, J. S.; Groeninckx, G.; Varughese, K. T.; Thomas, S. Rheological behaviour of thermoplastic elastomers from polypropylene/acrylonitrile−butadiene rubber blends: effect of blend ratio, reactive compatibilization and dynamic vulcanization. *Polymer* **1999**, *40*, 4325−4344.
(50) Mojarrad, A.; Jahani, Y.; Barikani, M. Investigation on the correlation between rheology and morphology of PA6/ABS blends using ethylene acrylate terpolymer as compatibilizer. *J. Appl. Polym. Sci.* **2011**, *120*, 2173−2182.
(51) Moly, K. A.; Oommen, Z.; Bhagawan, S. S.; Groeninckx, G.; Thomas, S. Melt rheology and morphology of LLDPE / EVA blends : Effect of blend ratio , compatibilization , and dynamic crosslinking. *J. Appl. Polym. Sci.* **2002**, *86*, 3210−3225.
(52) Aravind, I.; Jose, S.; Ahn, K. H.; Thomas, S. Rheology and morphology of polytrimethylene terephthalate/ethylene propylene diene monomer blends in the presence and absence of a reactive compatibilizer. *Polym. Eng. Sci.* **2010**, *50*, 1945−1955.
(53) Comyn, J.; Blackley, D. C.; Harding, L. M. Contact angles of liquids on films from emulsion adhesives, and correlation with the durability of adhesive bonds to polystyrene. *Int. J. Adhes. Adhes.* **1993**, *13*, 163−171.
(54) Kumar, K. D.; Bhowmick, A. K.; Tsou, A. H. Influence of aging on autohesive tack of brominated isobutylene-co-p-methylstyrene (BIMS) rubber in the presence of phenolic resin tackifier. *J. Adhes.* **2008**, *84*, 764−787.
(55) Kumar, K. D.; Tsou, A. H.; Bhowmick, A. K. Interplay between bulk viscoelasticity and surface energy in autohesive tack of rubber-tackifier blends. *J. Polym. Sci., Part B: Polym. Phys.* **2010**, *48*, 972−982.
(56) Owens, D. K.; Wendt, R. C. Estimation of the surface free energy of polymers. *J. Appl. Polym. Sci.* **1969**, *13*, 1741−1747.
(57) Maroufkhani, M.; Katbab, A. A.; Liu, W.; Zhang, J. Polylactide (PLA) and acrylonitrile butadiene rubber (NBR) blends: The effect of ACN content on morphology, compatibility and mechanical properties. *Polymer* **2017**, *115*, 37−44.
(58) Alanalp, M. B.; Durmus, A. Quantifying Microstructural, Thermal, mechanical and solid-state viscoelastic properties of polyolefin blend type thermoplastic elastomer compounds. *Polymer* **2018**, *142*, 267−276.

https://dx.doi.org/10.1021/acsomega.0c00423
ACS Omega 2020, 5, 12789−12808